Myoblast Sheet Can Prevent the Impairment of Cardiac Diastolic Function and Late Remodeling After Left Ventricular Restoration in Ischemic Cardiomyopathy

Shunsuke Saito,[1] Shigeru Miyagawa,[1] Taichi Sakaguchi,[1] Yukiko Imanishi,[1] Hiroko Iseoka,[1] Hiroyuki Nishi,[1] Yasushi Yoshikawa,[1] Satsuki Fukushima,[1] Atsuhiro Saito,[1] Tatsuya Shimizu,[2] Teruo Okano,[2] and Yoshiki Sawa[1,3]

Background. Impairment of diastolic function and late remodeling are concerns after left ventricular restoration (LVR) for ischemic cardiomyopathy. This study aims to evaluate the effects of combined surgery of myoblast sheets (MS) implantation and LVR.

Methods. Rat myocardial infarction model was established 2 weeks after left anterior descending artery ligation. They were divided into three groups: sham operation (n=15; group sham), LVR by plicating the infracted area (n=15; group LVR), and MS implantation with LVR (n=15; group LVR+MS).

Results. Serial echocardiographic study revealed significant LV redilatation and decrease of ejection fraction 4 weeks after LVR in group LVR. MS implantation combined with LVR prevented those later deteriorations of LV function in group LVR+MS. Four weeks after the operation, a hemodynamic assessment using a pressure-volume loop showed significantly preserved diastolic function in group LVR+MS; end-diastolic pressure (LVR vs. LVR+MS: 9.0±6.6 mm Hg vs. 2.0±1.0 mm Hg, $P<0.05$), end-diastolic pressure-volume relationship (LVR vs. LVR+MS 42±23 vs. 13±6, $P<0.05$). Histological examination revealed cellular hypertrophy and LV fibrosis were significantly less and vascular density was significantly higher in group LVR+MS than in the other two groups. Reverse transcription polymerase chain reaction demonstrated significantly suppressed expression of transforming growth factor-beta, Smad2, and reversion-inducing cysteine-rich protein with Kazal motifs in group LVR+MS.

Conclusions. MS implantation decreased cardiac fibrosis by suppressing the profibrotic gene expression and attenuated the impairment of diastolic function and the late remodeling after LVR. It is suggesting that MS implantation may improve long-term outcome of LVR for ischemic heart disease.

Keywords: Ischemic cardiomyopathy, Left ventricular restoration, Regenerative therapy, Myoblast sheet, Diastolic function.

(*Transplantation* 2012;93: 1108–1115)

Ischemic heart disease is one of the leading causes of death and disability in most of the industrialized countries and recognized as a major public health issue. Progression to end-stage heart failure involves massive loss of cardiomyocyte, massive fibrosis, and progressive remodeling of the ventricles. Left ventricular (LV) volume reduction surgery or LV restoration (LVR) surgery has been introduced as a surgical treatment of patients with dilated LV and chronic heart failure (*1*, *2*), and has been shown to reduce the LV volume, increase the ejection fraction, and improve ventricular function (*3*, *4*).

The authors declare no funding or conflicts of interest.

[1] Department of Cardiovascular Surgery, Osaka University Graduate School of Medicine, Suita, Osaka, Japan.

[2] Institute of Advanced Biomedical Engineering and Science, Tokyo Women's Medical University, Tokyo, Japan.

[3] Address correspondence to: Yoshiki Sawa, M.D., Department of Cardiovascular Surgery, Osaka University Graduate School of Medicine (E1), 2-2 Yamada-Oka, Suita, Osaka 565-0871, Japan.

E-mail: sawa@surg1.med.osaka-u.ac.jp

S.S. participated in research design, the performance of the research, data analysis, and the writing of the manuscript; T.S. participated in research design and data analysis; S.M. participated in research design and data analysis, and the writing of the manuscript; Y.I. performed quantitative analysis of engrafted myoblasts survival; H.I. performed histological analysis of engrafted myoblasts survival; H.N. participated in the performance of the research; Y.Y. participated in the performance of the research; S.F. participated in the performance of the research; A.S. participated in research design and data analysis; T.S. contributed to the development of the temperature-responsive culture dish and cell sheet implantation technique; T.O. contributed to the development of the temperature-responsive culture dish and cell sheet implantation technique; and Y.S. participated in research design, data analysis, and the writing of the manuscript.

Received 28 June 2011. Revision requested 20 July 2011.

Accepted 10 February 2012.

ISSN: 0041-1337/12/9311-1108

DOI: 10.1097/TP.0b013e31824fd803

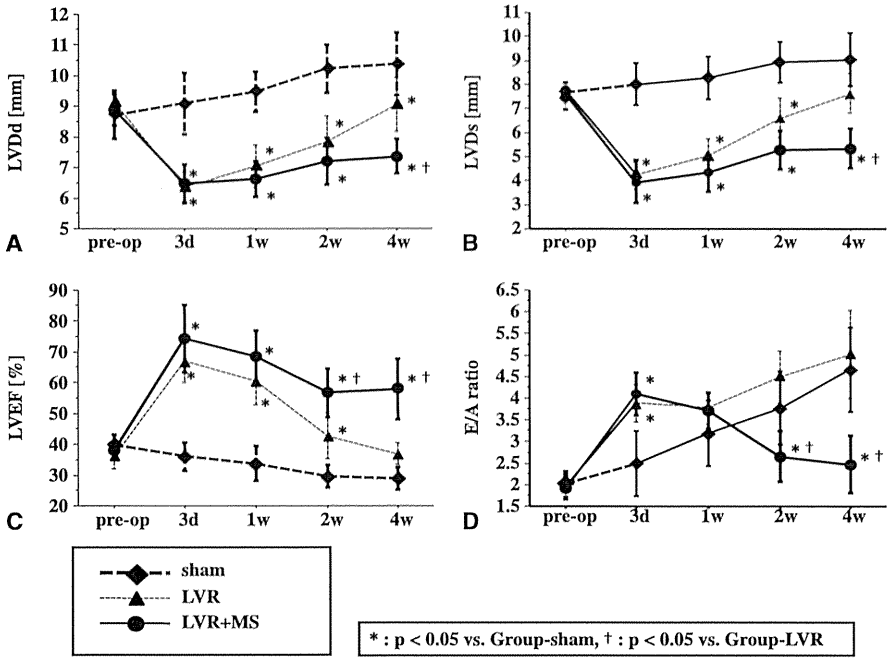

FIGURE 1. Serial echocardiographic study revealed significant decrease in left ventricular chamber size and significant increase in left ventricular ejection fraction by left ventricular restoration (LVR) in group LVR and in group LVR+ myoblast sheets (MS). However, gradual redilatation of left ventricular chamber and decrease of ejection fraction was observed in group LVR. Those later deteriorations were prevented in group LVR+MS, and the differences in chamber size and ejection fraction were significant between group LVR and group LVR+ MS 4 weeks after the operation. Changes in echocardiographic parameters before and after the operation. (A) Left ventricular dimension at end-diastole (LVDd), (B) left ventricular dimension at end-systole (LVDs), (C) Left ventricular ejection fraction (LVEF), (D) mitral valve E/A ratio. *P0.05 vs. group sham; †P0.05 vs. group LVR.

However, impairment of diastolic function and late remodeling are great concerns after LVR for ischemic cardiomyopathy (*5–7*), and the long-term effect of LVR is still controversial. Although LVR that is performed together with coronary artery bypass grafting (CABG) has been suggested to reduce the rate of hospitalization and improve ventricular function to a greater degree than CABG alone on the basis of a small, nonrandomized, case-control study (*8*), recently conducted multicenter, nonblinded, randomized trial (the Surgical Treatment for Ischemic Heart Failure [STICH] trial) have revealed that LVR does not improve the symptoms, exercise tolerance, rate of death, or hospitalization in patients with ischemic heart disease and severe LV dysfunction compared with CABG alone (*5*).

On the other hand, cell transplantation into impaired myocardium, also known as cellular cardiomyoplasty, has been investigated (*9*, *10*). Recently, we have developed a new cell delivery method by the means of cell sheet, in which autologous skeletal myoblasts were transplanted in sheet form, and reported that this method was effective especially in the attenuation of LV dilatation and the improvement of LV diastolic function (*11–14*). On the basis of these findings, we hypothesized that skeletal myoblast sheet (MS) implantation may attenuate the disadvantageous effects and enhance the advantageous effects of LVR. Using a rat model of chronic myocardial infarction model, we investigated whether MS implantation combined with LVR can attenuate the redilatation and diastolic dysfunction of LV after LVR.

RESULTS

Changes in Cardiac Function by LVR and LVR Combined With MS

Two weeks after left anterior descending coronary artery (LAD) ligation, severe dilatation of the LV chamber and severe asynergy of the anterior wall were observed in all the rats. By excluding the large akinetic or dyskinetic area of the LV anterior wall, LV dimension at end-diastole (LVDd) and end-systole (LVDs) significantly decreased and left ventricular ejection fraction (LVEF) significantly increased in group LVR and in group LVR+MS 3 days after treatment (Fig. 1). However, gradual LV redilatation and decrease of LVEF were observed in group LVR. MS implantation combined with LVR attenuated those later deteriorations of LV function significantly in group LVR+MS (Fig. 1). Mitral valve *E/A* ratio showed significant restrictive pattern after LVR. In group LVR, the restrictive pattern progressed even further with time. However, addition of the MS implantation attenuated the progression of the restrictive pattern (Fig. 1).

Hemodynamic Improvement by LVR Combined With MS

Table 1 shows the results of the hemodynamic study by cardiac catheterization 4 weeks after the second operation. The basic hemodynamic indices revealed that LV end-diastolic pressure (EDP) and the time constant of isovolumic relaxation (τ) were significantly lower in group LVR+MS than in group LVR or group sham. Load-independent parameters measured by pressure-volume loop analysis revealed that end-systolic pressure (ESP) volume relationship was significantly higher in group LVR+MS than in the other two groups. EDP volume relationship (EDPVR) was significantly lower in group LVR+MS than in the other two groups.

Histological Impact of the MS on the Failing Heart

Figure 2 shows the typical cross section of the whole hearts 4 weeks after the operation from each group. Severe dilatation of the LV chamber and thinning of the LV wall were observed in group sham (Fig. 2A). In group LVR, although infracted area was excluded and smaller than that in group sham, LV chamber was markedly dilated (Fig. 2B). Also severe dilatation of the right ventricular chamber was observed. In group LVR+MS, the size of the LV chamber and the thickness of the LV wall were well preserved compared

TABLE 1. Hemodynamic indices 4 weeks after the operation

Group	Sham	LVR	LVR+MS
Basic hemodynamic indices			
HR (bpm)	219 ± 37	206 ± 20	231 ± 32
ESP (mm Hg)	60.9 ± 7.7	63.0 ± 13.9	73.0 ± 11.3[a]
EDP (mm Hg)	5.1 ± 2.2	9.0 ± 6.6	2.0 ± 1.0[a,b]
τ (msec)	21.3 ± 2.4	19.8 ± 2.2	14.4 ± 1.2[a,b]
Load independent parameters analyzed by pressure-volume loop			
ESPVR (mm Hg/ml)	1896 ± 906	1364 ± 661	4722 ± 2416[a,b]
EDPVR (/ml)	50 ± 36	42 ± 23	13 ± 6[a,b]
PRSW (mm Hg)	37.1 ± 24.3	33.0 ± 24.2	45.2 ± 32.7

[a] $P < 0.05$ vs. group sham.
[b] $P < 0.05$ vs. Group-LVR.
HR, heart rate; ESP, end-systolic pressure; EDP, end-diastolic pressure; τ, time constant of isovolumic relaxation; ESPVR, end-systolic pressure-volume relationship; EDPVR, end-diastolic pressure-volume relationship; PRSW, preload-recruitable stroke work.

with the other groups (Fig. 2C). The LV wall thickness was significantly larger in group LVR+MS than in the other two groups (vs. group sham and group LVR, $P<0.05$) (Fig. 3A). The degree of cardiac fibrosis was significantly smaller in group LVR+MS than in the other two groups (vs. group sham and group LVR, $P<0.05$) (Figs. 3B and 4A–C). Myocyte size was also significantly smaller in group LVR+MS than in the other two groups (vs. group sham and group LVR, $P<0.05$) (Figs. 3C and 4D–F). Vascular density of the LV lateral wall, the area where MS were applied in group LVR+MS, was significantly higher in group LVR+MS than in the other two groups (vs. group sham and group LVR, $P<0.05$) (Figs. 3D and 4G–I).

Suppression of Probrotic Agent Gene Expression by MS

Reverse transcription polymerase chain reaction analysis 4 weeks after the second operation revealed significantly suppressed expression of the profibrotic gene transforming growth factor-beta (TGF-β), Smad2, and reversion-inducing cysteine-rich protein with Kazal motifs (RECK) in group LVR+MS than in the other two groups (vs. group sham and group LVR, $P<0.05$) (Fig. 5A–C).

FIGURE 2. Cross section of the whole hearts 4 weeks after the operation from each group (hematoxylin-eosin staining). (A) group sham, (B) group LVR, (C) group LVR + MS.

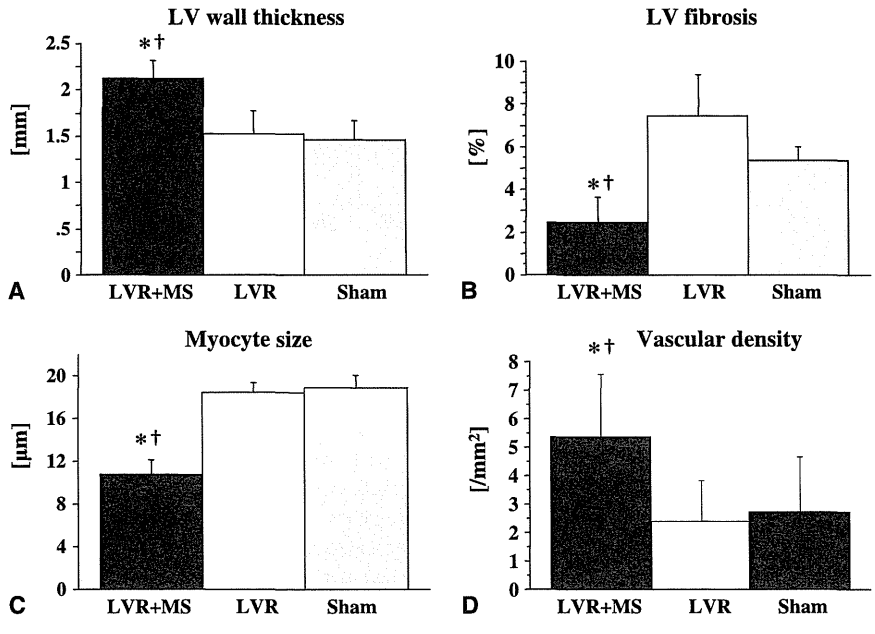

FIGURE 3. The left ventricular (LV) wall thickness was significantly larger in group left ventricular restoration (LVR)+myoblast sheets (MS) than in the other two groups 4 weeks after the operation (A). The degree of cardiac fibrosis (B) and myocyte size (C) were also significantly smaller in group LVR+MS than in the other two groups. The vascular density in the LV lateral wall, where MS were applied in group LVR+MS, were significantly higher in group LVR+MS than in the other two groups (D).

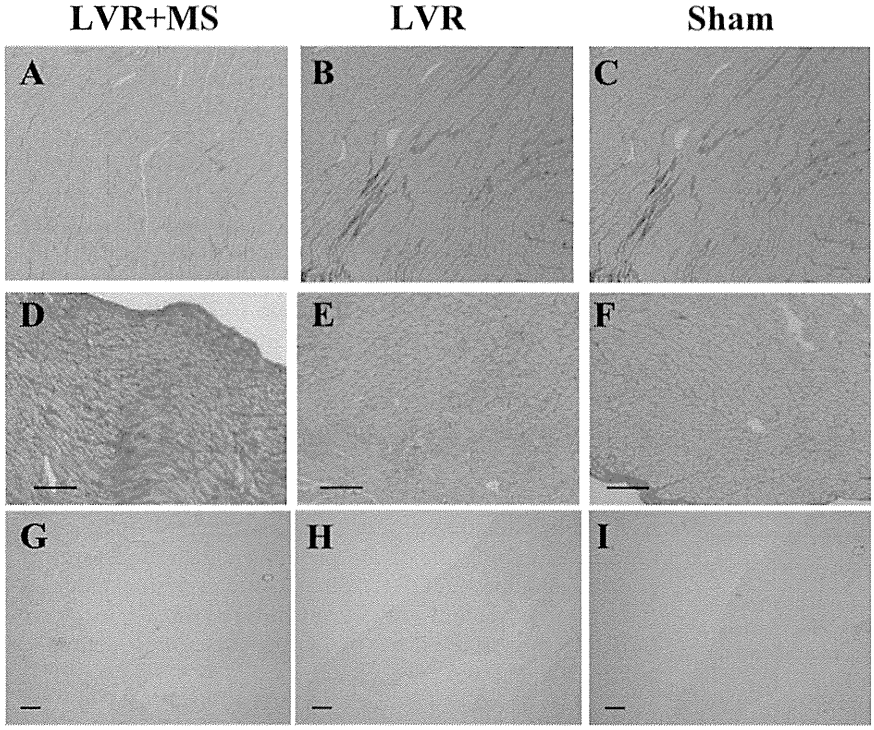

FIGURE 4. Picrosirius-red staining of myocardium from noninfarcted regions (A, B, C) and periodic acid-Schiff-stained myocardium from noninfarcted regions (D, E, F, bar=200 μm). Picrosirius-red staining of myocardium from noninfarcted regions. Sections of myocardium stained with antibody to von Willebrand factor (G, H, I, bar=300 μm).

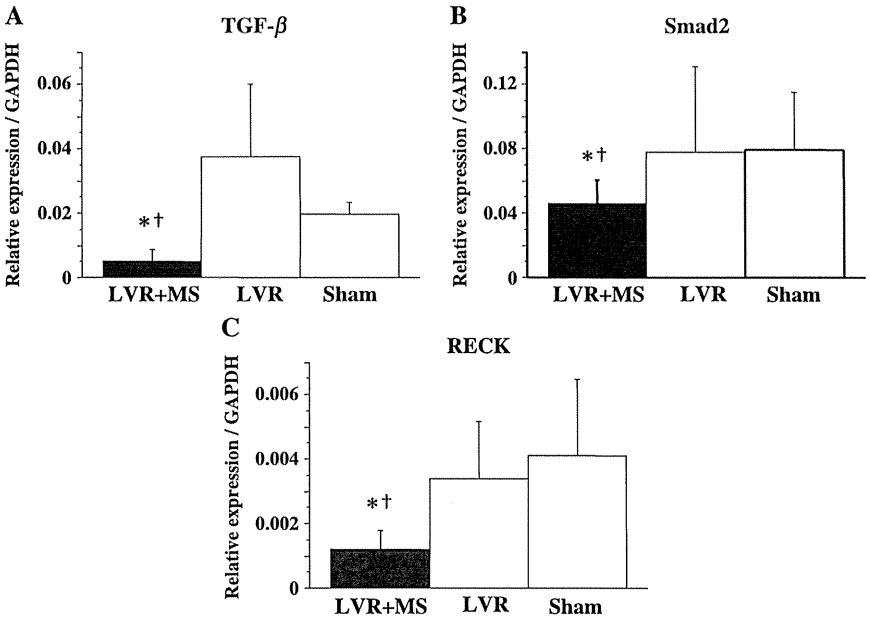

FIGURE 5. Reverse transcription polymerase chain reaction (RT-PCR) analysis 4 weeks after the second operation revealed significantly suppressed expression of the profibrotic gene transforming growth factor-beta (TGF-β) (A), Smad2 (B), and RECK (C) in group left ventricular restoration (LVR)+myoblast sheets (MS) than in the other two groups.

Engrafted Cell Survival

To evaluate the survival of engrafted cell on the recipient LV, MS made from male rats were implanted on the female LV, and surviving cell numbers were examined by detecting the Y chromosome-specific and gender consensus genes. To confirm the accuracy of the measurements, MS made from known numbers of male myoblasts were implanted on the LV wall of a female rat ex vivo, and a standard curve was prepared to determine the ratio of male cells to female cells and the relationship to the number of male cells. The correlation coefficient for the standard curve was 0.9716, indicating a significant correlation. The number of surviving engrafted cells was calculated using this standard curve (*15*). The number of cells detected on the day of implantation was approximately 64% of the engrafted cells (five layers of MS, with 3.0×10^6 myoblasts in each sheet). Surviving cells decreased to 69% of those in day 0. Although the number continued to decrease with time, 13% of those cells were still surviving on the LV wall 4 weeks after MS implantation (Fig. 6A).

Immunostaining of the green fluorescent protein (GFP) revealed that myoblasts sheets made from GFP transgenic rats

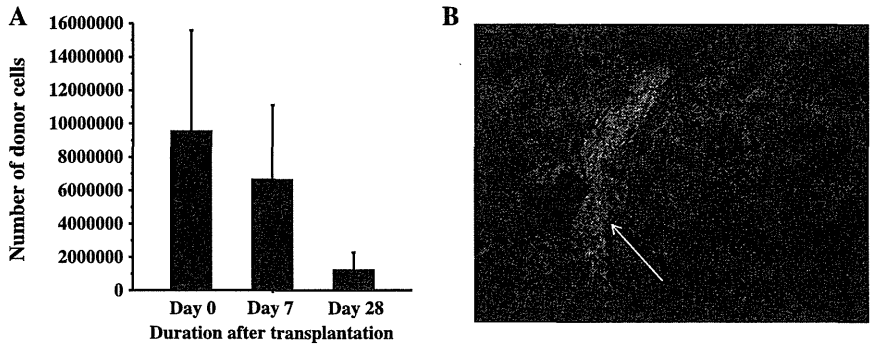

FIGURE 6. Survival of donor cells in recipient hearts. (A) Number of surviving engrafted cells in recipient hearts. Although the number of donor cells decreased with time, the surviving engrafted cells were still detectable 28 days after transplantation. (B) Immunostaining of the green fluorescent protein. Transplanted myoblast sheets were still detectable 28 days after the surgery.

were still detectable on the epicardium of LV wall 28 days after implantation (Fig. 6B).

DISCUSSION

Impairment of diastolic function and late remodeling are concerns after LVR for ischemic cardiomyopathy (*5–7*). Dor et al. (*6*) have reported the late redilatation of LV after LVR in their clinical experiences, and Nishina et al. (*16*) have developed a rat model that reproduces this clinical situation, in which model an infracted area of the LV anterior wall was simply plicated. Although LV configuration and function improved after the operation, LV chamber gradually redilated and LV function decreased, and the initial improvement almost disappeared in 4 weeks.

Using this same model, we implanted the skeletal MS concomitantly with LVR to investigate the ability of MS to overcome the drawbacks of the LVR. In this study, MS implantation attenuated the LV redilatation and decrease in EF after LVR. It was also shown by echocardiographic study and pressure-volume loop analysis that MS attenuated the impairment of diastolic function after LVR. Histological examination revealed that MS induced the angiogenesis in the myocardium where they were applied, and decreased the degree of myocardial fibrosis. MS controlled the gene expression that may regulate the myocardial fibrosis (TGF-β, Smad2, and RECK), and suppressed myocardial fibrosis. The number of viable myoblasts implanted on the LV wall concomitantly with LVR decreased with time, but they were still detectable on the LV wall 28 days after implantation. The surviving cells detected on the LV wall 28 days after transplantation were only 13% of those detected on the day of transplantation. However, to enhance the survivability and effectiveness of implanted cells, we have developed new additional therapy such as transfection of the gene for hepatocyte growth factor (HGF) (*17*) or omentum flap (*18*) combined with cell transplantation, and reported the efficacies of these additional therapies in the previous studies.

The mechanism of recovery of cardiac function by autologous MS are considered as combination of restoration of the LV wall by the MS, that is "girdling effect," and biological effects of the cytokines such as stromal-derived factor 1 (SDF-1), HGF, and vascular endothelial growth factor (VEGF) paracrined from sheet-shaped autologous myoblasts, that is "paracrine effect." SDF-1 is known to mobilize and recruit stem cells and leads to neovascularization (*19, 20*) and is secreted in skeletal muscle tissue (*21*). HGF is an angiogenic and antifibrotic factor (*22*), and VEGF is also a potent angiogenic factor (*23*). In the previous reports with animal models, we have demonstrated that the gene expressions of SDF-1, HGF, and VEGF were significantly higher in the hearts treated with MS than in hearts treated with myoblasts injection or with medium injection (*11, 14, 24*). As results of those enhanced gene expression, the hearts treated with MS showed higher number of hematopoietic stem cells in the treated area (*11*), greater vascularity (*11, 12, 14*), decreased cardiac fibrosis (*11–14, 24*), decreased apoptotic cells (*13*), and increased proliferative cells (*13*). Moreover, those effects were enhanced as the number of transplanted MS increased (*14*). Sekiya et al. (*14*) reported that the effect of the MS was maximally enhanced when it was implanted on the impaired myocardium in five layers, compared with three or one layer. Based on these data and experiences in our own laboratory, we chose the skeletal myoblasts as donor of cell sheets in this study, and decided the cell number and the layer number of the MS. In this study, we reconfirmed that angiogenesis was induced and fibrosis was suppressed by MS. It is considered that the angiogenesis enhanced the myocardial microcirculation and improved the myocardial ischemia, and resulted in attenuation of myocardial fibrosis and late remodeling. Instead of the well-known key factors secreted by MS such as SDF-1, HGF, and VEGF, we investigated the other signals that are known to control the degree of tissue fibrosis such as TGF-β, Smad, and RECK. TGF-β is a known profibrotic cytokine that has been demonstrated to induce cardiac fibrosis (*25*). The effect of TGF-β in the heart is primarily mediated though Smad2 phosphorylation (*26*). The TGF-β-Smad pathway seems to be involved in the activation of collagen-gene promoter sites, increasing DNA translation of collagen I. In this study, it was clearly proved that MS suppress the TGF-β-Smad pathway leading to the attenuation of cardiac fibrosis. RECK is known to be one of the inhibitors of metalloproteinases (*27*) and believed to be an important regulator of cardiac extracellular matrix. Although in this study we could not evaluate the matrix metalloproteinase (MMP) and tissue inhibitors of metalloproteinase activity, MS may activate the MMP acting through the suppression of RECK, leading to the reduction of fibrosis. It was shown for the first time that MS suppressed the degree of myocardial fibrosis by regulating those signals. The mechanisms by which MS regulate those signals remain to be investigated.

We also revealed that LV wall thickness was maintained and LV dilatation was attenuated by MS after LVR. From Laplace's law, this might have led to decrease in

LV wall stress and attenuation of the myocardial cellular hypertrophy.

In our previous study, we reported that MS increased elastin in the myocardium where the MS were implanted, and this might have contributed to the improvement in diastolic function (*14*). In this study, all the data acquired from echocardiography (mitral *E/A* ratio), catheter study (LVEDP, τ, and EDPVR), and histological study (fibrosis) revealed improvement of diastolic function by the MS.

One of the unique points of this study, compared with the previous studies with skeletal MS, was that the MS were applied to the viable area of the myocardium in this study. One of the most important mechanisms of the myocardial improvements by MS is considered paracrine effect of cytokines secreted from the skeletal myoblast. From this point of view, it is anticipated that the greater the number of the viable cells in the area of myocardium where the MS is attached, the greater the effect of the MS. This study is different from the previous studies in the point that the impaired myocardium was excluded by surgical LVR and the skeletal MS were attached to the remaining viable area of the myocardium. In the preliminary experiment of this study, we have also included the "MS only group" in the study groups. As reported in the previous studies, MS showed a certain effects and prevented the deterioration of the heart function compared with sham group. However, the comparisons between the group LVR+MS and "MS only group" were complicated because the conditions of the myocardium in which the MS were applied were different, so we excluded this group from the final design of this study.

Using the rat LVR model, other additional treatments such as administration of angiotensin-converting enzyme inhibitor (*28*), chymase inhibitor (*29*), or transplantation of fetal cardiomyocyte by needle injection (*30*) were reported to prevent the late remodeling after LVR in some extent. Not like the single medical treatments mentioned above, MS implantation affects on cardiac function by integrated pathway of angiogenesis, antifibrosis, mechanical unloading of the LV wall stress, and possibly other unknown mechanisms. MS implantation is supposed to be more effective than single medical treatment. As a cell delivery method, it is known that direct intramyocardial injection has several disadvantages, including cell loss caused by leakage of injected cells from the myocardium, poor survival of the grafted cells, myocardial damage after mechanical injury by the needle, and subsequent acute inflammation. MS implantation is a useful method to overcome these disadvantages, and we have reported the superiority of the myocardial sheets implantation to needle injection (*11–13*).

This study has some limitations. In this rat model, the area of myocardial infarction is not identical in all the rats 2 weeks after ligating the coronary artery, and thus the size of the LV and the degree of impairment of diastolic function are not identical in all the rats after LVR. Second, the surgery for excluding the infarction was carried out by imbrication stitches, and this is different from the actual procedure in the clinical setting, excision and re-sculpting of the left ventricle as described by Dor et al. (*6*). Additionally, we chose rats with large akinetic area as a myocardial infarction model and aggressively plicated this area to reproduce "the failing situation" after LVR. This situation may not be directly applied to clinical settings. However, we consider that the effectiveness of MS to attenuate impairment of diastolic function and late remodeling after LVR was shown by this model. We also recognize some limitations in our study with regard to the analysis of the mechanisms in which the MS reduce the cardiac fibrosis. Although we have demonstrated the enhanced gene expression of smad and RECK, further study is needed to analyze the level of gene expression of collagens, MMPs, and tissue inhibitors of metalloproteinases to show the activation of Smad2 and RECK protein.

In conclusion, skeletal MS implantation attenuated the impairment of diastolic function and the late remodeling after LVR in rat myocardial infarction model. It is suggested that MS implantation may improve the long-term outcome of LVR for ischemic heart disease.

MATERIALS AND METHODS

Animal Care

All experimental procedures and protocols used in this investigation were reviewed and approved by the institutional animal care and use committee and are in accordance with the National Institutes of Health Guide for the Care and Use of Laboratory Animals (NIH Publication No. 85-23, Revised 1996).

Isolation of Myoblasts and Construction of MS

Myoblasts were isolated from the skeletal muscle of the anterior tibialis from 3-week-old male Lewis rats and cultured as previously described (*11–14*). They were dissociated from the culture dishes with trypsin-ethylenediaminetetraacetic acid and reincubated on 35-mm temperature-responsive culture dishes (UpCell, Cellseed, Tokyo, Japan) at 37°C, with cell number adjusted to 3.0×10^6 per dish. More than 70% of these cells were actin-positive and 40% to 50% were desmin-positive (*14*). After 24 hr, the dishes were incubated at 20°C for 30 min. During that time, the MS detached spontaneously to generate free-floating, monolayer cell sheets. After detachment, the area of the sheets decreased to 1.00±0.05 cm^2, while the thickness increased to 100±10.0 μm (*14*). For the immunostaining of the engrafted MS, myoblasts were isolated from GFP transgenic Lewis rats and made into cell sheets in the same way as described earlier.

Myocardial Infarction Model

Eight-week-old male Lewis rats were used (220–250 g; Seac Yoshitomi Ltd. Fukuoka, Japan). The rats were anesthetized with ketamine (90 mg/kg) and Xylazine (10 mg/kg), and myocardial infarction was induced by ligation of LAD under mechanical ventilation. Two weeks after the ligation, baseline cardiac functions were measured by echocardiography, and rats that fulfill the following criteria were selected for further experiment: large akinetic or dyskinetic area in the anterior wall of the LV, LVDd 9.0±1.0 mm, and LVEF 35%±5%. For the quantitative study of the engrafted cell fate, 8-week-old female Lewis rats were used and myocardial infarction model was made in the same way as described earlier.

Experimental Groups

Male rats were randomized into three groups: 15 rats underwent only rethoracotomy (group sham), 15 underwent LVR (group LVR), and 15 underwent LVR, which was immediately followed by MS implantation (group LVR+MS). In group LVR and group LVR+MS, LVR was performed as follows: three to four mattress stitches with 7-0 polypropylene sutures were placed just onto the border line between infarcted and intact myocardium, and the infarcted myocardium was excluded (*16*). In group LVR+MS, five layers of MS were attached directly to the intact myocardium without sutures subsequently to LVR. After detachment from the temperature-responsive dish, each sheet was picked up individually and applied to the surface of the heart. After 3 to 5 min, subsequent sheets were applied and a total of five layers of MS were implanted. All the female rats underwent implantation of MS made from male rats concomitantly with LVR for the engrafted cell fate analysis. Additionally, three rats underwent implantation of the MS made from GFP positive

myoblasts after LVR in the same way as group LVR+MS for immunostaining of implanted MS.

Echocardiography

LV functions of all the treated rats were monitored by echocardiography at baseline (2 weeks after LAD ligation), 3 days, 1 week, 2 weeks, and 4 weeks after the second operation. Echocardiography was performed with a SONOS 5500 (Agilent Technologies, Palo Alto, CA) using a 12-MHz annular array transducer under anesthesia with inhalation of isoflurane. The hearts were imaged in short-axis 2D views at the level of the papillary muscles, and the LVDs and LVDd were determined. LVEF was calculated by Pombo's method, as EF (%)=$\{(LVDd^3-LVDs^3)/LVDd^3\}\times 100$. All the echocardiographic studies were performed by a single investigator who was blinded to the treatment groups and the results were agreed by all the other investigators.

Hemodynamic Study and Data Analysis

Four weeks after the second operation, after the last echocardiographic study, all the rats were ventilated again. Re-re-thoracotomy was performed and the LV apex was dissected carefully to minimize hemorrhaging. A silk thread was placed under the inferior vena cava just above the diaphragm to change the LV preload. After a purse string suture was attached to the LV apex with 7-0 polypropylene, the conductance catheter (Unique Medical Co., Tokyo, Japan) was inserted through the LV apex toward the aortic valve along the longitudinal axis of the LV cavity and then fixed. A Miller 1.4 Fr pressure-tip catheter (SPR-719, Millar Instruments, Houston, TX) was also inserted from the LV apex and fixed. The conductance system and the pressure transducer controller (Integral 3 [VPR-1002], Unique Medical Co.) were set as previously reported (*31*). The pressure-volume loops and intracardiac electrocardiogram were monitored online, and the conductance, pressure, and intracardiac electrocardiographic signals were analyzed with Integral version 3 software (Unique Medical Co.) (*31*). Under stable hemodynamic conditions, the baseline indices were initially measured and then the pressure-volume loop was drawn during the inferior vena cava occlusion and analyzed.

The following indices were calculated as the baseline LV function: heart rate, ESP, EDP, and τ. ESP volume relationship and EDPVR were determined by pressure-volume loop analysis as load-independent measures of the LV function. All the catheter studies were performed by a single investigator who was blinded to the treatment groups and the results were agreed by all the other investigators.

Histological Study

After all measurements were finished, the rats were killed for histological study. In eight rats from each group, LV myocardial specimens were obtained and fixed with 10% buffered formalin and embedded in paraffin. Hematoxylin-eosin staining was performed for the measurement of the ventricular wall thickness. The thickness of the ventricular wall was measured at two points from the LV posterior area and two points from the interventricular septum, and results were expressed as the average of the four points. Picrosirius red staining was performed to detect myocardial fibrosis. Myocardial fibrosis was expressed as percent fibrosis, the fraction of red-stained area in total myocardium, with results obtained from 10 fields per section per animal from LV lateral and posterior wall. Also periodic acid-Schiff staining was performed to examine the degree of cardiomyocyte hypertrophy. Myocyte size was determined by point-to-point perpendicular lines drawn across the cross-sectional area of the cell at the level of the nucleus. The results were expressed as the average diameter of 40 myocytes randomly selected from the LV lateral and posterior wall. To label vascular endothelial cells, so that blood vessels could be counted, immunohistochemical staining for factor VIII-related antigen was performed according to a modified protocol. We used EPOS-conjugated antibody to factor VIII-related antigen coupled with HRP (Dako EPOS Anti-Human von Willebrand Factor/HRP, Dako) as primary antibody. The stained vascular endothelial cells were counted under a light microscope. Results were expressed as the number of blood vessels/mm^2.

Measurement Probrotic Agent Gene Expression 4 Weeks After LVR and MS Implantation

In the remaining seven rats from each group, the myocardium from the LV lateral wall, the area where MS were applied in group LVR+MS, were also stored in RNAlater solution (QIAGEN, Hilden, Germany). Total RNA was extracted with the RNeasy mini kit (QIAGEN), and relative levels of RNA transcripts were measured by the real-time quantitative reverse transcription polymerase chain reaction technique using the ABI PRISM 7700 Sequence Detection System. The measurement of the mRNA expression of TGF-β, Smad2, and RECK was performed in triplicate. The results are expressed after normalization for glyceraldehydes-phosphate dehydrogenase.

Quantitative and Histological Evaluation of Engrafted Cell Survival

Intact hearts from female Lewis rats were collected, freed of the right ventricular free wall, and transplanted with MS made from known numbers (3.0×10^2, 3.0×10^3, 3.0×10^4, 3.0×10^5, 3.0×10^6, or 3.0×10^7, n=3 each) of male Lewis rats myoblast. Samples were homogenized and analyzed for the levels of *sry* and *il2*, which are Y chromosome-specific and gender consensus genes, respectively. An estimate of the fraction of donor cells was calculated as $2\times$ *sry*/*il2*$\times 100$, and standard curves were constructed to determine the myoblast number from the percentage of male cells (*15*). The amount of donor myoblasts was measured on the day of MS implantation (n=5), 7 days (n=6), and 28 days (n=5) after implantation. Genomic DNA was prepared using an Allprep kit (Qiagen). Quantitative polymerase chain reaction of *sry* and *il2* was performed with 1.2 μg of DNA using Taqman universal polymerase chain reaction master mix (Applied Biosystems) according to the manufacturer's instructions and an ABI PRISM7700 sequence detection system (Applied Biosystems).

To evaluate the surviving engrafted cell histologically, five layers of MS made from myoblasts of GFP transgenic Lewis rats were implanted on the LV of Lewis rats. They were killed 28 days after the surgery.

Data Analysis

All data were expressed as the mean±standard error of mean and subjected to analysis of variance (ANOVA). Time-course data were first analyzed by using repeated-measurements two-way ANOVA, and the other numeric data were analyzed by using one-way ANOVA. If significance was found, posthoc comparisons were performed. Findings were considered significant at P less than 0.05.

REFERENCES

1. Dor V, Saab M, Coste P, et al. Left ventricular aneurysm: A new surgical approach. *Thorac Cardiovasc Surg* 1989; 37: 11.
2. Athanasuleus CL, Stanley AWH Jr, Buckberg GD. Restoration of contractile function in the enlarged left ventricle by exclusion of remodeled akinetic anterior segment: Surgical strategy, myocardial protection, and angiographic results. *J Card Surg* 1998; 13: 418.
3. Athanasuleus CL, Buckberg GD, Stanley AWH, et al. Surgical ventricular restoration in the treatment of congestive heart failure due to post-infarction ventricular dilation. *J Am Coll Cardiol* 2004; 44: 1439.
4. Menicanti L, Castelvecchio S, Ranucci M, et al. Surgical therapy for ischemic heart failure: Single-center experience with surgical anterior ventricular restoration. *J Thorac Cardiovasc Surg* 2007; 134: 433.
5. Jones RH, Velazquez EJ, Michler RE, et al. Coronary bypass surgery with or without surgical ventricular reconstruction. *N Engl J Med* 2009; 360: 1.
6. Dor V, Sabatier M, Di Donato M, et al. Efficacy of endoventricular patch plasty in large postinfarction akinetic scar and severe left ventricular dysfunction: Comparison with a series of large dyskinetic scars. *J Thorac Cardiovasc Surg* 1998; 116: 50.
7. Sinatra R, Macrina F, Braccio M, et al. Left ventricular aneurysmectomy; comparison between two techniques; early and late results. *Eur J Cardiothorac Surg* 1997; 12: 291.
8. Prucz RB, Weiss ES, Patel ND, et al. Coronary artery bypass grafting with or without surgical ventricular restoration: A comparison. *Ann Thorac Surg* 2008; 86: 806.
9. Taylor DA, Atkins BZ, Hungspreugs P, et al. Regenerating functional myocardium: Improved performance after skeletal myoblast transplantation. *Nat Med* 1998; 4: 929.
10. Orlic D, Kajstura J, Chiment S, et al. Bone marrow cells regenerate infracted myocardium. *Nature* 2001; 410: 701.
11. Memon IA, Sawa Y, Fukushima N, et al. Repair of impaired myocardium by means of implantation of engineered autologous myoblast sheets. *J Thorac Cardiovasc Surg* 2005; 130: 1333.
12. Kondoh H, Sawa Y, Miyagawa S, et al. Longer preservation of cardiac performance by sheet-shaped myoblast implantation in dilated cardiomyopathic hamsters. *Cardiovasc Res* 2006; 69: 466.

13. Hata H, Matsumiya G, Miyagawa S, et al. Grafted skeletal myoblast sheets attenuate myocardial remodeling in pacing-induced canine heart failure model. *J Thoracic Cardiovasc Surg* 2006; 132: 918.
14. Sekiya N, Matsumiya G, Miyagawa S, et al. Layered implantation of myoblast sheets attenuates adverse cardiac remodeling of the infracted heart. *J Thorac Cardiovasc Surg* 2009; 138: 985.
15. Kitagawa-Sakakida S, Tori M, Li Z, et al. Active cell migration in retransplanted rat cardiac allografts during the course of chronic rejection. *J Heart Lung Transplant* 2000; 19: 584.
16. Nishina T, Nishimura K, Yuasa S, et al. Initial effects of the left ventricular repair by placation may not last long in a rat ischemic cardiomyopathy model. *Circulation* 2001; 104: I-241.
17. Miyagawa S, Sawa Y, Taketani S, et al. Myocardial regeneration therapy for heart failure. Hepatocyte growth factor enhances the effect of cellular cardiomyoplasty. *Circulation* 2002; 105: 2556.
18. Shudo Y, Miyagawa S, Fukushima S, et al. Novel regenerative therapy using cell-sheet covered with omentum flap delivers a huge number of cells in a porcine myocardial infarction model. *J Thorac Cardiovasc Surg* 2011; 142: 1199.
19. Askari AT, Unzek S, Penn MMS, et al. Effect of stromal-cell-derived factor 1 on stem-cell homing and tissue regeneration in ischemic cardiomyopathy. *Lancet* 2003; 362: 97.
20. Miyagawa S, Roth M, Saito A, et al. Tissue-engineered cardiac constructs for cardiac repair. *Ann Thorac Surg* 2011; 91: 320.
21. Ratajczak MZ, Peier S, Janowska WA, et al. Expression of functional CXCR4 by muscle satellite cells and secretion of SDF-1 by muscle-derived fibroblasts is associated with the presence of both muscle progenitors in bone marrow and hematopoietic stem/progenitor cells in muscles. *Stem Cells* 2003; 21: 363.
22. Taniyama Y, Morishita R, Aoki M, et al. Angiogenesis and antifibrotic action by hepatocyte growth factor in cardiomyopathy. *Hypertension* 2002; 40: 47.
23. Shimizu T, Okamoto H, Chiba S, et al. VEGF-mediated angiogenesis is impaired by angiotensin type 1 receptor blockade in cardiomyopathic hamster hearts. *Cardiovasc Res* 2003; 58: 203.
24. Hoashi T, Matsumiya G, Miyagawa S, et al. Skeletal myoblast sheet transplantation improves the diastolic function of a pressure-overloaded right heart. *J Thorac Cardiovasc Surg* 2009; 138: 460.
25. Nakajima H, Nakajima HO, Salcher O, et al. Atrial but not ventricular fibrosis in mice expressing a mutant transforming growth factor-beta(1) transgene in the heart. *Circ Res* 2000; 86: 571.
26. Pokharel S, Rasoul S, Roks AJ, et al. *N*-acelyl-Ser-Asp-Lys-Pro inhibits phosphorylation of Smad2 in cardiac fibrosis. *Hypertension* 2002; 40: 155.
27. Oh J, Takahashi R, Kondo S, et al. The membrane-anchored MMP inhibitor RECK is a key regulator of extracellular matrix integrity and angiogenesis. *Cell* 2001; 107: 789.
28. Nomoto T, Nishina T, Miwa S, et al. Angiotensin-converting enzyme inhibitor helps prevent late remodeling after left ventricular aneurysm repair in rats. *Circulation* 2002; 106: I-115.
29. Kanemitsu H, Takai S, Tsuneyoshi H, et al. Chronic chymase inhibition preserves cardiac function after left ventricular repair in rats. *Eur J Cardiothorac Surg* 2008; 33: 25.
30. Sakakibara Y, Tambara K, Lu F, et al. Combined procedure of surgical repair and cell transplantation for left ventricular aneurysm: An experimental study. *Circulation* 2002; 106: I-193.
31. Sato T, Shishido T, Kawada T, et al. ESPVR of in situ rat left ventricle shows contractility-dependent curvilinearity. *Am J Physiol* 1998; 274: 1429.

Biochemical and Biophysical Research Communications 425 (2012) 859–865

Contents lists available at SciVerse ScienceDirect

Biochemical and Biophysical Research Communications

journal homepage: www.elsevier.com/locate/ybbrc

Intracoronary artery transplantation of cardiomyoblast-like cells from human adipose tissue-derived multi-lineage progenitor cells improve left ventricular dysfunction and survival in a swine model of chronic myocardial infarction

Hanayuki Okura [a,b], Ayami Saga [b], Mayumi Soeda [b], Shigeru Miyagawa [c], Yoshiki Sawa [c], Takashi Daimon [d], Akihiro Ichinose [e], Akifumi Matsuyama [a,e,f,*]

[a] The Center for Medical Engineering and Informatics, Osaka University, 2-2 Yamada-oka, Suita, Osaka 565-0879, Japan
[b] Department of Somatic Stem Cell Therapy and Health Policy, Institute of Biomedical Research and Innovation, Foundation for Biomedical Research and Innovation, 2-2 Minatojima-minamimachi, Chuo-ku, Kobe, Hyogo 650-0047, Japan
[c] Department of Surgery, Osaka University Graduate School of Medicine, 2-2 Yamada-oka, Suita, Osaka 565-0879, Japan
[d] Division of Biostatistics, Hyogo College of Medicine, 1-1 Mukogawa-cho, Nishinomiya, Hyogo 663-8501, Japan
[e] Department of Plastic Surgery, Kobe University Hospital, 7-5-2 Kusunoki-cho, Chuo-ku, Kobe, Hyogo, Japan
[f] RIKEN Program for Drug Discovery and Medical Technology Platforms, 1-7-22 Suehiro-cho, Tsurumi-ku, Yokohama, Kanagawa 230-0045, Japan

ARTICLE INFO

Article history:
Received 12 July 2012
Available online 7 August 2012

Keywords:
Cellular cardiomyoplasty
ADMPCs
Myocardial infarction
Transplantation

ABSTRACT

Transplantation of human cardiomyoblast-like cells (hCLCs) from human adipose tissue-derived multi-lineage progenitor cells improved left ventricular function and survival of rats with myocardial infarction. Here we examined the effect of intracoronary artery transplantation of human CLCs in a swine model of chronic heart failure. Twenty-four pigs underwent balloon-occlusion of the first diagonal branch followed by reperfusion, with a second balloon-occlusion of the left ascending coronary artery 1 week later followed by reperfusion. Four weeks after the second occlusion/reperfusion, 17 of the 18 surviving animals with severe chronic MI (ejection fraction <35% by echocardiography) were immunosuppressed then randomly assigned to receive either intracoronary artery transplantation of hCLCs hADMPCs or placebo lactic Ringer's solution with heparin. Intracoronary artery transplantation was followed by the distribution of DiI-stained hCLCs into the scarred myocardial milieu. Echocardiography at post-transplant days 4 and 8 weeks showed rescue and maintenance of cardiac function in the hCLCs transplanted group, but not in the control animals, indicating myocardial functional recovery by hCLCs intracoronary transplantation. At 8 week post-transplantation, 7 of 8 hCLCs transplanted animals were still alive compared with only 1 of the 5 control ($p = 0.0147$). Histological studies at week 12 post-transplantation demonstrated engraftment of the pre DiI-stained hCLCs into the scarred myocardium and their expression of human specific alpha-cardiac actin. Human alpha cardiac actin-positive cells also expressed cardiac nuclear factors; nkx2.5 and GATA-4. Our results suggest that intracoronary artery transplantation of hCLCs is a potentially effective therapeutic strategy for future cardiac tissue regeneration.

1. Introduction

End-stage heart failure remains a major cause of death worldwide, mainly due to myocardial ischemia. Cardiac transplantation and mechanical support using implantation of the left ventricular assist system (LVAS) were established as the ultimate means of support for these patients [1,2]. However, these treatment entities have certain limitations including donor shortage, rejection, and LVAS durability, and alternative strategies are needed in such circumstances.

Cellular cardiomyoplasty was developed as a new approach to restore normal heart function, [3,4] using a variety of cell types [3–5]. Mesenchymal stem cells (MSC) seem particularly advantageous for cellular therapy in general because they are multipotent, potentially immune privileged [6]. MSC also proliferate rapidly and differentiate into cardiomyogenic cells [7–10]. MSC can be isolated from human adipose tissue, which can be resected easily and safely in most patients [11,12]. In fact, we have reported that adipose tissue-derived multilineage progenitor cells (ADMPCs), which met the criteria as mesenchymal stem cells [13], can differentiate into hepatocytes both *in vitro* and *in vivo* [14,15]. Recently, we demonstrated that human cardiomyoblast-like cells (hCLCs) from human adipose tissue-derived multi-lineage progenitor cells transplanted into rats with chronic myocardial infarction reversed wall thinning

* Corresponding author at: The Center for Medical Engineering and Informatics, Osaka University, 2-2 Yamada-oka, Suita, Osaka 565-0879, Japan.
E-mail address: akifumi-matsuyama@umin.ac.jp (A. Matsuyama).

0006-291X/$ - see front matter © 2012 Elsevier Inc. All rights reserved.
http://dx.doi.org/10.1016/j.bbrc.2012.08.004

in the scarred area with the engrafted cells forming a thick stratum, and that the hCLCs reversed left ventricular dysfunction in the long term and survival of rats with experimentally-induced myocardial infarction [16].

The present study is an extension to the above study and was designed to accelerate the clinical application of hCLCs. Specifically, we examined in pre-/non-clinical studies the effects of hCLCs transplantation on cardiac dysfunction and on long-term survival with swine chronic myocardial infarction model. We also documented the histological regeneration of damaged myocardium after transplantation of hCLCs *in vivo*.

2. Materials and methods

2.1. Adipose tissue

Adipose tissue samples were resected from five human subjects during plastic surgery (all females, age, 20–60 years) as excess discards. Ten to 50 g of subcutaneous adipose tissue were collected from each subject after obtaining of informed consent. The protocol was approved by the Review Board for Human Research of Kobe University Graduate School of Medicine, Osaka University Graduate School of Medicine and Foundation for Biomedical Research and Innovation.

2.2. Isolation of hADMPCs and preparation of hCLCs

Human adipose tissue-derived multi-lineage progenitor cells (hADMPCs) were prepared as described previously [13–17]. After passaging 5 to 6 times, the hADMPCs were replated and treated with 0.1% dimethyl sulfoxide (DMSO) (Cryoserve, GE Healthcare Biosciences, Uppsala, Sweden) for 48 h.

2.3. Reverse transcriptase–polymerase chain reaction

Total RNA was isolated from hADMPCs and cardiomyoblasts using an RNAeasy kit (Qiagen, Hilden, Germany). After treatment with DNase, cDNA was synthesized from 500 ng total RNA using Superscript III reverse transcriptase RNase H minus (Invitrogen, Carlsbad, CA). Real-time PCR was performed using the ABI Prism 7900 Sequence Detection System (Applied Biosystems, Foster City, CA). 20X Assays-on-Demand™ Gene Expression Assay Mix for *nkx2.5* (Hs00231763_m1), *islet-1* (Hs00158126_m1), *GATA-4* (Hs00171403_m1), *alpha-cardiac actin* (Hs01109515_m), *cardiac troponin I* (Hs00165957_m1), *myosin light chain* (*MLC*) (Hs00166405_m1), *myosin heavy chain* (*MHC*) (Hs00411908_m1) and *glyceraldehyde-3-phosphate dehydrogenase* (*GAPDH*) (Hs99999905_m1) were obtained from Applied Biosystems. TaqMan® Universal PCR Master Mix, No AmpErase® UNG (2X), was also purchased from Applied Biosystems. Reactions were performed in quadruplicate and the mRNA levels were normalized relative to human GAPDH expression. Then the fold-inductions of hCLCs were compared to hADMPCs.

2.4. Animal model of myocardial infarction and cell transplantation

Five weeks before transplantation, the first diagonal branch (D1; #9) of the coronary arteries of 24 pigs (8-week-old female, 30.5 ± 0.7 kg, mean ± standard error of the mean) was balloon-occluded for 60 min followed by reperfusion, (Fig. 1A). One week later, the left ascending coronary artery of the same animals was balloon-occluded just proximal of the first septal branch divergence (#6), followed by reperfusion (Fig. 1A). To rescue the better baseline survivals and to obtain severe old myocardial infarction swine model, two separate reperfused infarcts one week apart were performed. From 5 days before cell transplantation to the end of the experiment, the swine received tacrolimus as an immunosuppressant (0.1 mg/kg/day intramuscularly) (Fig. 1B) as previously reported [18] with modification. Four weeks after the second occlusion/reperfusion (day 0), we examined 17 animals with chronic severe MI (ejection fraction <35% by echocardiography) of only 18 survivors. The tacrolimus-immunosuppressed chronic MI swine were randomly assigned to receive intracoronary transplantation of hCLCs (3×10^5 cells/mL concentration of cell

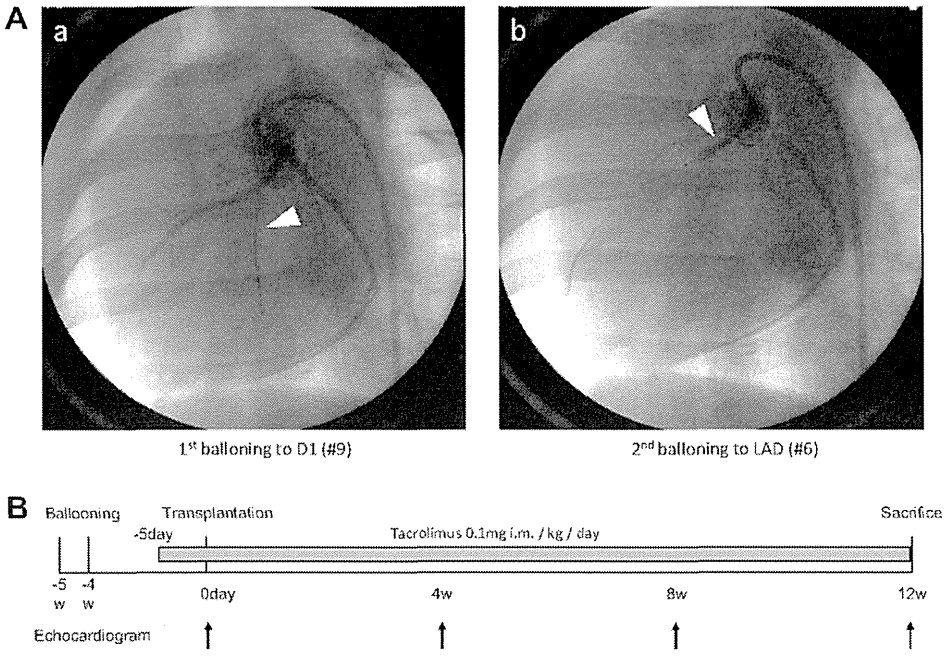

Fig. 1. Study protocol and angiographic demonstration of transient coronary artery occlusion. (A) Five weeks before transplantation, the first diagonal branch (D1; #9) of the coronary arteries was balloon-occluded followed by reperfusion (a, arrowhead). One week later, the left ascending coronary artery of the same animals was balloon-occluded just proximal of the first septal branch divergence (#6), followed by reperfusion (b, arrowhead). (B) From 5 days before cell transplantation to the end of the experiment, the swine received tacrolimus as an immunosuppressant. At day 0, 17 animals with chronic severe MI were applied for the experiment.

Table 1
Cardiocytic induction of hCLCs.

	Fold induction	
	Mean	SE
nkx2.5	2.49	1.02
islet-1	1.32	0.36
GATA-4	6.84	1.47
Alpha-Cardiac actin	1.46	0.22
Cardiac troponin I	2.36	0.47
Myosin light chain	1.89	0.49
Myosin heavy chain	109.89	6.13

suspension, 1 mL/kg cell suspension was transplanted.) ($n = 8$), hADMPCs (3×10^5 cells/mL concentration of cell suspension, 1 mL/kg cell suspension was transplanted.) ($n = 4$), or placebo lactic Ringer's solution with heparin ($n = 5$), at 4 weeks after the second occlusion/reperfusion. Transplantation procedure was performed as following, the transarterial catheter was placed in the left coronary artery, and then the cell-suspensions or placebo control solutions were transplanted into LAD (#6). The Osaka University Graduate School of Medicine Standing Committee on Animals approved all experimental protocols.

2.5. Assessment of swine cardiac function and histological analysis

Cardiac ultrasound studies were performed before cell-transplantation and at 4, 8 and 12 weeks after transplantation using a VIVID 7 system (GE Healthcare Biosciences, Uppsala, Sweden) and the data at the day transplantation, 4- and 8-week-after transplantation were applied for the statistical analysis. The studies were shown as M-mode with short axis view observed from left fifth intracostal space.

For histological analysis, the swine hearts were dissected out at the end of the experiment and immediately fixed overnight in 4% paraformaldehyde and processed for embedding in paraffin wax. Sections were cut at 3-μm thickness, deparaffinized and then rehydrated through a graded ethanol series into distilled water. The sections were then immersed in Target Retrieval Solution (Dako, Glostrup, Denmark) and boiled, followed by cooling at room temperature for 20 min. Sections were incubated overnight with 10% blocking solution (Nacalai tesque) in TBS-T, and then in a humidity chamber for 16 h at 4 °C with mouse monoclonal antibodies to human alpha-cardiac actin (American Research Products., Belmont, MA), human myosin heavy chain (MHC) (mouse monoclonal anti-human myosin heavy chain cardiac antibody, Cat: 05-833., Upstate, NY) and CD34 (ab81289 [EP373Y], Abcom) diluted in blocking solution, followed by Alexa Fluor 488-labeled anti- IgG (Molecular Probes, Eugene, OR) with counter DAPI-staining. Hematoxylin and eosin stain, Masson trichrome stain and Sirius red stain were also performed. The stained all slides were viewed on a BioZero laser scanning microscope (Keyence, Osaka, Japan). The scarred area percentages of the middle portion and apex side of LV were calculated by area stained blue with Masson's trichrome staining/total of 10 each independent sections using software Dynamic Cell Count (Keyence, Osaka, Japan).

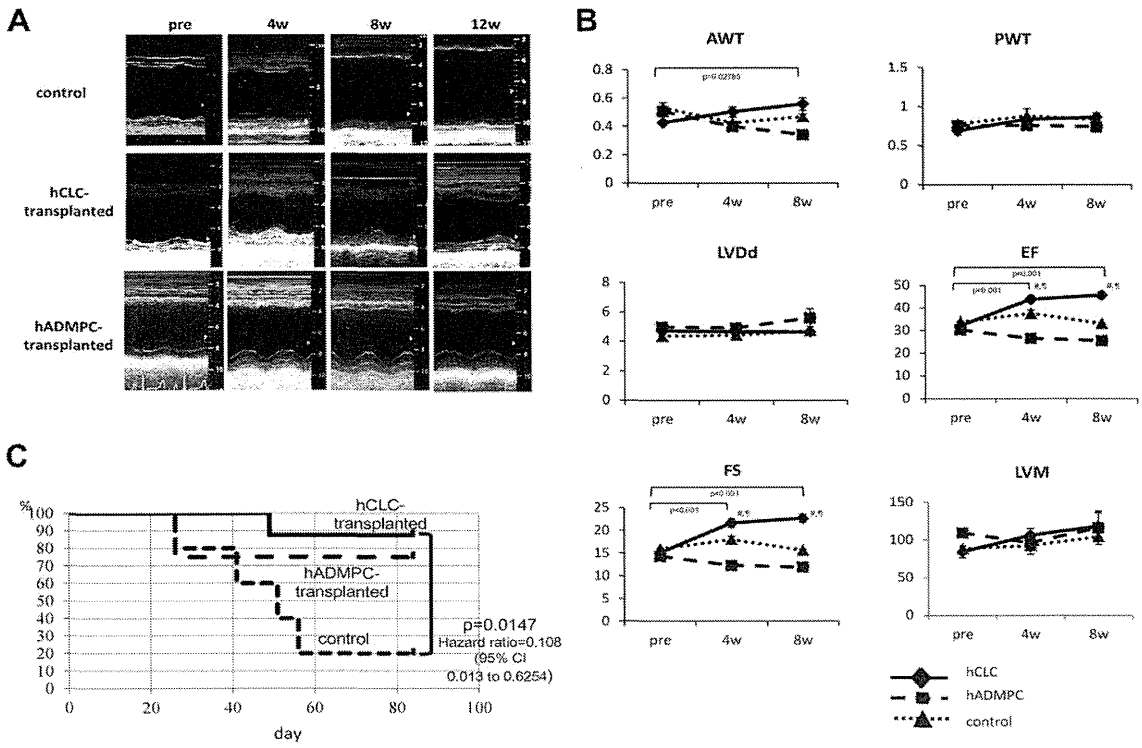

Fig. 2. Effects of hCLCs transplantation on cardiac function and survival rate. (A) In the hCLCs transplanted group, M-mode echocardiography showed improved wall motion within 4 weeks of transplantation. In contrast, worsening of the wall motion was noted in the mock-transplanted control swine. (B) Anterior wall thickness (AWT), ventricular ejection fraction (EF) and fractional shortening (FS) improved significantly in the hCLCs transplanted group, as confirmed by echocardiography. In the hCLCs transplanted swine, cardiac functions were recovered from transplantation to the end of the study. In the hADMPCs transplanted swine, cardiac functions were maintained from transplantation to the end of the study. In contrast, worsening of these cardiac function parameters was noted after mock-transplantation. The left ventricular diastolic dimension (LVDd) was maintained during the course of the experiment in hCLCs transplanted swine, but increased in the control groups. Posterior wall thickness (PWT) and left ventricular mass (LVM) showed no significant difference in the groups. Solid lines and squares indicated the transplanted group and the dashed lines and open squares indicated the control group. The symbol # indicated $p < 0.01$ hCLCs -transplanted vs control and indicated $p < 0.01$ hADMPC-transplanted vs control, respectively. Bars indicated mean ± standard error of the mean (SEM). (C) Effect of hCLCs transplantation ($n = 8$), hADMPCs transplantation ($n = 4$) and lactic Ringer's solution injection ($n = 5$) on long-term survival rates of swine. Kaplan–Meier survival curve analysis demonstrated significant difference in the survival rates between the hCLCs group and the lactic Ringer's solution group.

2.6. Statistical analysis

Longitudinal changes between groups were tested with the use of mixed-model repeated-measures analysis of variance, with adjustment for baseline values. When the overall P value for the main effect of group or time, or interaction between group and time was less than 0.05, the post hoc multiple comparisons with the use of the single-step adjustment method as implemented by Hothorn et al. were performed [19]. Survival curves were constructed by the Kaplan–Meier method and survival among groups was compared using the Log-Rank test (StatMate III for Windows, Atoms, Tokyo).

3. Results

3.1. Cardiocytic commitment of hADMPCs into hCLCs

The potential for hADMPCs to commit into CLCs was evaluated from the mRNA expression of several cardiocytic markers by quantitative reverse transcriptase-PCR before and after DMSO induction, as follows: *islet-1* is a cardiac stem cell marker; *nkx2.5* and *GATA-4* are transcription factors required for subsequent cardiac differentiation; and *alpha-cardiac actin*, *myosin light chain* (*MLC*), and *myosin heavy chain* (*MHC*) are markers of cardiocytic commitment (Table 1). After induction, hADMPCs expressed all markers with increment, indicating that hADMPCs could be successfully committed into cells of the cardiac lineage, hCLCs.

3.2. Effects of hCLCs transplantation on cardiac function and survival rate

Cardiac function was assessed by echocardiography. Four weeks after intracoronay transplantation of hCLCs, wall motion was improved but not in the placebo group (Fig. 2A). The wall motion of control swine worsened at 12 weeks after transplantation, while the improved motion was maintained after the hCLCs transplant (Fig. 2A). In the early post-transplantation period, there was no significant difference in left ventricular diastolic dimension (LVDd) between hCLCs -transplanted swine and the control. During the course of the study, LVDd exacerbated gradually in the control swine while it did not change significantly in the transplant swine (Fig. 2B). Likewise, the left ventricular ejection fraction (EF) and fractional shortening (FS) improved in the implanted group, but not in control swine (Fig. 2B). After hCLCs transplantation via left anterior descending (#6), the anterior wall thickness improved in the implanted group, but not in control swine. These results indicate that intracoronary transplantation of hCLCs resulted in recovery of cardiac function.

The Kaplan–Meier survival curves showed higher long-term survival rates for the hCLCs transplanted group than the control (Fig. 2C). Notably, only 1 of 8 swine died after transplantation of hCLCs. Survival at 12 weeks after transplantation was significantly higher in the hCLCs group (87.5%) than the control group (20%, 1 of 5) (Log-rank test: $p = 0.0147$. Hazard ratio = 0.108: 95% CI 0.013 to 0.625). These results suggest that transplantation of hCLCs

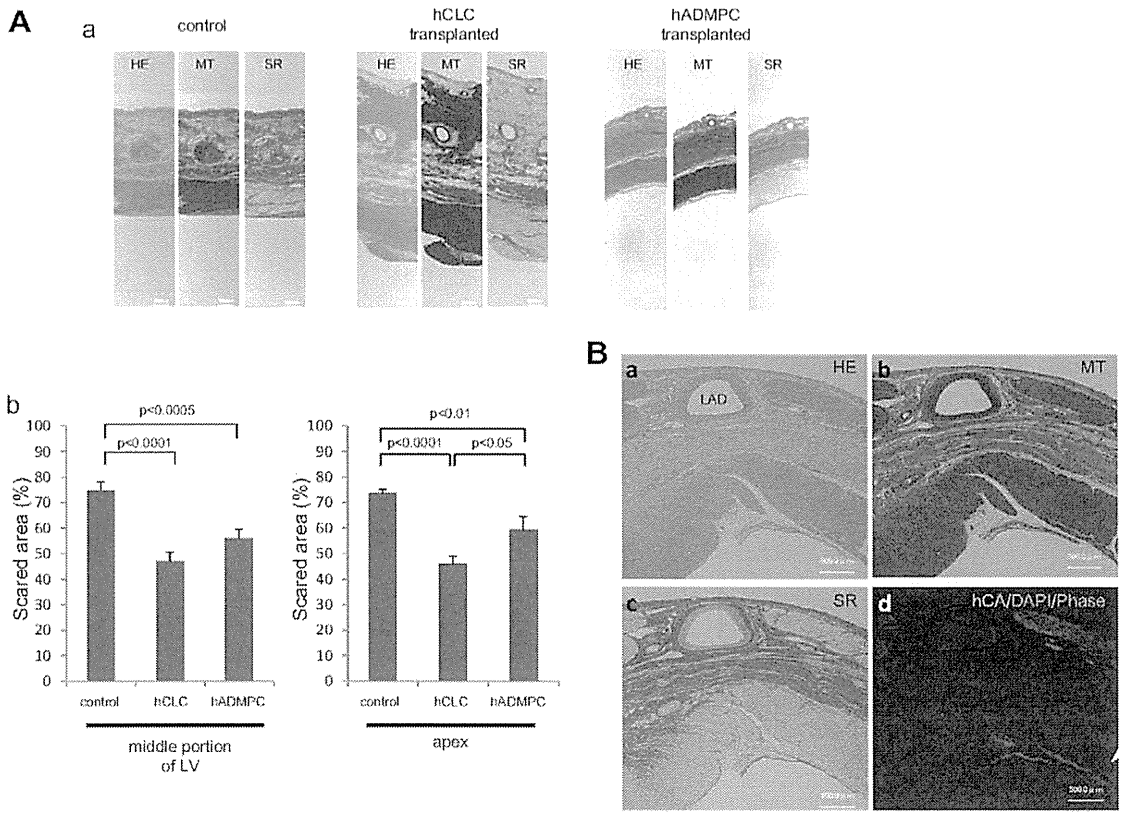

Fig. 3. Effects of hCLCs transplanted via coronary artery on cardiac structure. (A) (a) Photomicrographs of representative myocardial sections of the scarred area stained with hematoxylin/eosin (HE), Masson trichrome (MT) and Sirius red (SR) in the hCLCs-, hADMPC-transplantation and mock-transplanted control groups. Transplantation of hCLCs improved myocardial wall thickness in the infarcted myocardium and resulted in the development of new cardiac muscles on the surface. Bars = 500 μm. HE; hematoxylin and eosin staining, MT; Masson trichrome staining, and SR; Sirius red staining. (b) The scarred area percentages of the middle portion and apex side of LV. The scarred area percentages of hCLCs-, hADMPC-transplantation and control groups were calculated by area stained blue with Masson's trichrome staining /total of 10 independent sections. The error bar indicated SEM. (B) Photomicrographs of representative myocardial sections of apical side of the anterior wall stained with HE (a), MT (b), SR (c) or phase contrast merge image of neighboring sections stained with anti-human alpha-cardiac actin (hCA; green), and DAPI as counter staining (d). In the HE-, MT-, and SR-stained sections, cardiac muscles were distributed on the scarred areas, and some parts of these muscles expressed human alpha-cardiac actin (green). Bars = 500 μm. LAD; left anterior descending.

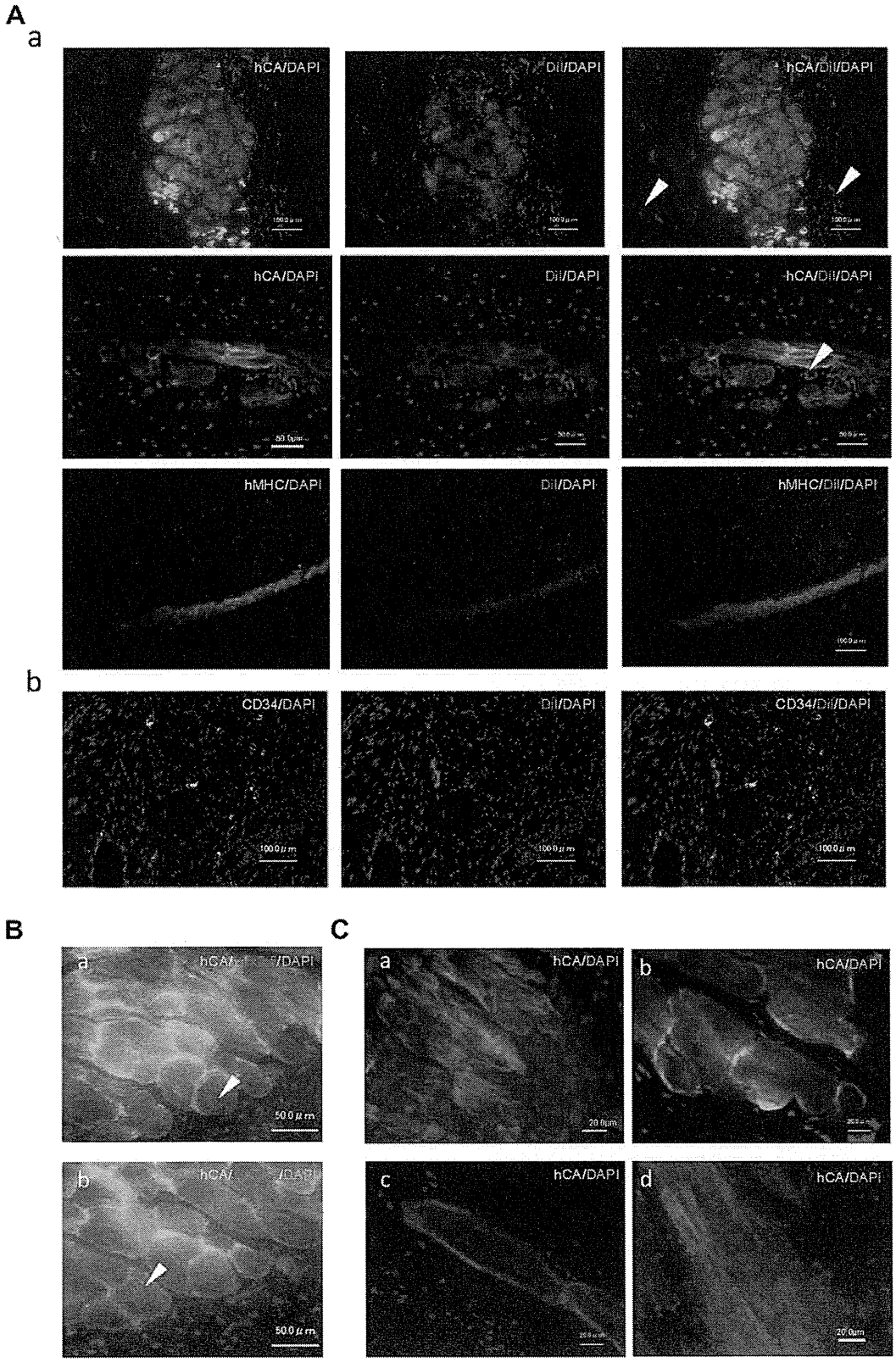

Fig. 4. hCLCs survive *in situ*. (A) (a) *In situ* survivals of the fluorescent DiI-prestained hCLCs into cardiomyocytes at 12-week- after transplantation. Note the presence of human alpha-CA positive cardiac muscle bundles or cells and that almost all cells exhibit DiI-fluorescence. Only minor part of DiI-positive cells did not express human alpha-CA (arrowheads). DiI-prestained cells were also positive for human myosin heavy chain (lower panel). (b) Survivals of hCLCs outside of vessel capillaries. The vessel capillaries were stained with anti-CD34 antibody and localization of DiI-positive cells were examined using fluoromicroscpy. DiI-positive cells exist outside of vessel capillaries which were stained with anti-CD34 antibody (B) Co-expression of human alpha-CA (green) and Nkx2.5 (purple) (a) or GATA-4 (purple) (b) in the nuclei of human alpha-CA positive cells. (C) Typical expression patterns of human alpha-CA on the cells. Human alpha-CA exhibited a brush pattern in oval cells (a), a spot pattern in cell-to-cell contact areas (b), as a sarcomeric structure beneath around the cell surface (c), and in a pattern resembling cardiomyocytes (d). Bars = 20 μm.

improves long-term survival rate of swine with heart failure induced by chronic myocardial infarction.

3.3. Effects of hCLCs transplantation on cardiac structure

Twelve weeks after transplantation, the treated swine were sacrificed and cardiac tissues prepared for histological examination for further analysis of cardiac structure and delineate the difference between hCLCs transplanted animals and controls (Fig. 3). Hematoxylin/eosin, Masson's trichrome and Sirius red staining showed the presence of a thin layer of cardiac muscles and massive fibrosis in the scarred anterior left ventricular wall of the control and hADMPCs transplanted swine (Fig. 3Aa). In contrast, the same staining techniques in hCLCs -transplanted swine showed significant thickening of the infarcted myocardium and layers of cardiomyocytes on the anterior ventricular wall (Fig. 3Aa). Next, to confirm the hCLCs could rescue from the fibrosis on cardiac structure, the scarred area percentages of the middle portion and apex side of LV were calculated. As shown in Fig. 3Ab, the percentage of scarred area of hCLCs -transplantation heart reduced compared to the control swine heart and hADMPC-transplanted one in both middle portion of LV and apex side.

3.4. hCLCs integrated in situ with the cardiac milieu

The *in situ* differentiation capacity of the implanted hCLCs into cardiomyocytes after grafting onto the scarred myocardium was assessed by immunohistochemical staining for human alpha-CA (Fig. 3B). Thin layers of cardiomyocytes were noted on the scarred myocardium by hematoxylin and eosin staining and Masson trichrome staining. Furthermore, clusters of human alpha-CA-positive cells were identified on the scarred myocardium (Fig. 3B; Green, arrowhead), indicating that hCLCs might integrate *in situ* with the cardiac milieu.

To confirm that the transplanted hCLCs survived *in situ*, we chased the fluorescent DiI-prestained hCLCs *in situ* 12 weeks after transplantation using histochemical technique. The top panel of Fig. 4Aa shows human alpha-CA positive cardiac muscle bundle and almost all cells of the bundle were DiI-fluorescent. The middle panel shows that all human alpha-CA-expressing cells were prestained DiI-fluorescent. DiI-prestained cells were also positive for human myosin heavy chain (Fig. 4Aa lower panel). On the other hand, DiI-positive cells exist outside of vessel capillaries which were stained with anti-CD34 antibody (Fig. 4Ab). Since cardiomyocytes are known to express the nuclear transcriptional factors; Nkx2.5 and GATA-4, we examined the expression of these molecules on human alpha-CA positive cells. The nuclei of human alpha-CA positive cells (green) expressed Nkx2.5 (purple) (Fig. 4Ba) and those of human alpha-CA positive cells (green) expressed GATA-4 (purple) (Fig. 4Bb), adding further confirmation that hCLCs might differentiate into cardiac marker positive cells.

The expression patterns of human alpha-CA on the cells were presented in Fig. 4C. The first pattern of human alpha-CA expression was the brushed pattern in oval-shaped cells (Fig. 4Ca). Alpha-CA also showed a spot pattern in the cell-to-cell contact areas (Fig. 4Cb). Resident alpha-CA-like immunoreactivity also appeared as sarcomeric structure beneath and around the cell surface (Fig. 4Cc). The fourth pattern of alpha-CA was cardiomyocyte structure-like pattern (Fig. 4Cd). These results indicate that hCLCs survive *in situ* and integrate into the cardiac milieu.

4. Discussion

There are several advantages to intracoronay transplantation of hCLCs for regeneration therapy. First, the source of adipose-derived cells is easily and safely accessible and large quantities of the cells can be obtained without serious ethical issues. Second, hCLCs can survive *in vivo* within the myocardial milieu. Finally, the reconstruction of a thick myocardial wall rescued cardiac dysfunction after chronic myocardial infarction and improved long-term survival in our swine model.

The choice of cell source is critical for realizing success in cellular therapy [19,20]. The adipose tissue is easily and safely accessible without serious ethical issues, and the cells can be obtained in large quantities since liposuction surgeries yield from 100 ml to >3 L of lipoaspirate tissue [21]. In the literature, isolation of cells from adipose tissue was first described by Bjorntorp et al. [22]. This procedure was then modified for the isolation of cells from human adipose tissue specimens [23–25]. In this context, Zuk et al. [11] reported the presence of cells with properties resembling those of mesenchymal stem cells resident in adipose tissue and they renamed the cell populations as adipose tissue-derived stromal/stem cells (ADSC). Recently, we have reported hADMPC as a novel cell population in human adipose tissue and indicated that these cells have stem cell features resembling mesenchymal stem cells including their ability to differentiate into cardiomyocytes in rat infracted cardiac milieu, into hepatocytes in rabbit hepatic milieu *in situ*, and into clusters of islet-like cells and hepatocytes *in vitro* [13–16]. Based on the above advantages, hADMPCs represent a potentially promising source of cells for cellular therapy, including patients with severe heart failure.

While the differentiation of ADSCs *in vitro* has been reported [26], only a few studies reported their differentiation into cardiomyocytes *in vivo* [27–29]. In one study, rat ADSCs were isolated and grown in intact monolayer sheets using temperature-responsive culture dishes. Placement of the rat ADSC sheets onto scarred myocardium in rats reduced the scarring and enhanced cardiac structure and function. Histological analysis demonstrated that the engrafted rat ADSC sheets grew to form a thickened layer that included newly formed vessels and few cardiomyocytes. In this context, Gimble et al. [20] suggested that hADSCs might secrete angiogenic factors. In our previous study, hCLCs survived within the rat myocardial milieu *in vivo*, as indicated by immunohistological results, suggesting that the newly developed myocardium could augment cardiac function.

As indicated in this study, transplantation of the hCLCs via the coronary artery resulted in the development of a new thick myocardial tissue, rescued cardiac dysfunction after MI in the swine model, and improved long-term survival rate compared to the control. Our findings suggest that hCLCs can be engrafted and survive within the myocardial infarct milieu, acquire phenotypic markers consistent with cardiomyocytic lineages, and have a positive impact on structural and functional endpoints. These are desirable outcomes for cardiac function and survival. Despite these encouraging results, much progress is needed to realize the hope of cell therapies for myocardial damage. First, delivery of the cell number to patients should be optimized for each given disease. Second, the risk–benefit based approach should be considered in the infracted or affected tissues after transplantation. Finally, the value and impact of hCLCs -transplantation should be confirmed in Investigational New Drug approval before embarking on clinical trials and applications.

In conclusion, we showed that the hCLCs were successfully engrafted into the scarred myocardium. The hCLCs -transplantation via the coronary artery also resulted in recovery of cardiac function and improved survival rate. Thus, transplantation of hCLCs in heart patients is a potentially effective therapeutic strategy for cardiac tissue regeneration within a few years.

Acknowledgments

This work was supported in part by a Grant-in-Aid for Akifumi Matsuyama from the Ministry of Health, Labor and Welfare

(MHLW) (http://www.mhlw.go.jp/ Grant No: H21-Nanchi-Ippan-219) and by a Grant-in Aid for Akifumi Matsuyama by the Program for Promotion of Fundamental Studies in Health Sciences of the National Institute of Biomedical Innovation (NIBIO) (http://www.nibio.go.jp/ Grant No: 09-19).

References

[1] S. Miyagawa, Y. Sawa, S. Taketani, et al., Myocardial regeneration therapy for heart failure hepatocyte growth factor enhances the effect of cellular cardiomyoplasty, Circulation 105 (2002) 2556–2561.
[2] S. Miyagawa, G. Matsumiya, T. Funatsu, et al., Combined autologous cellular cardiomyoplasty using skeletal myoblasts and bone marrow cells for human ischemic cardiomyopathy with left ventricular assist system implantation: report of a case, Surg. Today 39 (2009) 133–136.
[3] D.A. Taylor, Cell-based myocardial repair: how should we proceed?, Int J. Cardiol. 95 (2004) S8–S12.
[4] J.C. Chachques, C. Acar, J. Herreros, et al., Cellular cardiomyoplasty: clinical application, Ann. Thorac. Surg. 77 (2004) 1121–1130.
[5] B.A. Pallante, J.M. Edelberg, Cell sources for cardiac regeneration – which cells and why, Am. Heart Hosp. J. 4 (2006) 95–97.
[6] R.C. Chiu, MSC immune tolerance in cellular cardiomyoplasty, Semin. Thorac. Cardiovasc. Surg. 20 (2008) 115–118.
[7] M.F. Pittenger, A.M. Mackay, S.C. Beck, et al., Multilineage potential of adult human mesenchymal stem cells, Science 284 (1999) 143–147.
[8] Y. Jiang, B.N. Jahagirdar, R.L. Reinhardt, et al., Pluripotency of mesenchymal stem cells derived from adult marrow, Nature 418 (2002) 41–49.
[9] M.F. Pittenger, B.J. Martin, Mesenchymal stem cells and their potential as cardiac therapeutics, Circ. Res. 95 (2004) 9–20.
[10] C. Toma, M.F. Pittenger, K.S. Cahill, B.J. Byrne, P.D. Kessler, Human mesenchymal stem cells differentiate to a cardiomyocyte phenotype in the adult murine heart, Circulation 105 (2002) 93–98.
[11] P.A. Zuk, M. Zhu, H. Mizuno, et al., Multilineage cells from human adipose tissue: implications for cell-based therapies, Tissue Eng. 7 (2001) 211–228.
[12] A.J. Katz, A. Tholpady, S.S. Tholpady, H. Shang, R.C. Ogle, Cell surface and transcriptional characterization of human adipose-derived adherent stromal (hADAS) cells, Stem Cells 23 (2005) 412–423.
[13] H. Komoda, H. Okura, C.M. Lee, et al., Reduction of *N*-glycolylneuraminic acid xenoantigen on human adipose tissue-derived stromal cells/mesenchymal stem cells leads to safer and more useful cell sources for various stem cell therapies, Tissue Eng. Part A 16 (2010) 1143–1155.
[14] H. Okura, H. Komoda, A. Saga, et al., Properties of hepatocyte-like cell clusters from human adipose tissue-derived mesenchymal stem cells, Tissue Eng. Part C Methods 16 (2010) 761–770.
[15] H. Okura, A. Saga, Y. Fumimoto, et al., Transplantation of human adipose tissue-derived multilineage progenitor cells reduces serum cholesterol in hyperlipidemic Watanabe rabbit, Tissue Eng. Part C Methods 17 (2011) 145–154.
[16] H. Okura, A. Matsuyama, C.M. Lee, et al., Cardiomyoblast-like cells differentiated from human adipose tissue-derived mesenchymal stem cells improve left ventricular dysfunction and survival in a rat myocardial infarction model, Tissue Eng. Part C Methods 16 (2010) 417–425.
[17] A. Saga, H. Okura, M. Soeda, et al., HMG-CoA reductase inhibitor augments the serum total cholesterol-lowering effect of human adipose tissue-derived multilineage progenitor cells in hyperlipidemic homozygous Watanabe rabbits, Biochem. Biophys. Res. Commun. 412 (2011) 50–54.
[18] H. Sahara, A. Shimizu, K. Setoyama, et al., Beneficial effects of perioperative low-dose inhaled carbon monoxide on pulmonary allograft survival in MHC-inbred CLAWN miniature swine, Transplantation 90 (2010) 1336–1343.
[19] T. Hothorn, F. Bretz, P. Westfall, Simultaneous inference in general parametric models, Biom. J. 50 (2008) 346–363.
[20] C.E. Murry, H. Reinecke, L.M. Pabon, Regeneration gaps: observations on stem cells and cardiac repair, J. Am. Coll. Cardiol. 47 (2006) 1777–1785.
[21] J.M. Gimble, A.J. Katz, B.A. Bunnel, Adipose-derived stem cells for regenerative medicine, Cir. Res. 100 (2007) 1249–1260.
[22] P. Bjorntorp, M. Karlsson, H. Pertoft, et al., Isolation and characterization of cells from rat adipose tissue developing into adipocytes, J. Lipid Res. 19 (1978) 316–324.
[23] S. Deslex, R. Negrel, C. Vannier, J. Etienne, G. Ailhaud, Differentiation of human adipocyte precursors in a chemically defined serum-free medium, Int. J. Obes. 11 (1987) 19–27.
[24] H. Hauner, G. Entenmann, M. Wabitsch, et al., Promoting effect of glucocorticoids on the differentiation of human adipocyte precursor cells cultured in a chemically defined medium, J. Clin. Invest. 84 (1989) 1663–1670.
[25] H. Hauner, M. Wabitsch, E.F. Pfeiffer, Differentiation of adipocyte precursor cells from obese and nonobese adult women and from different adipose tissue sites, Horm. Metab. Res. Suppl. 19 (1988) 35–39.
[26] A.M. Parker, A.J. Katz, Adipose-derived stem cells for the regeneration of damaged tissues, Expert Opin. Biol. Ther. 6 (2006) 567–578.
[27] S. Rangappa, J.W. Entwistle, A.S. Wechsler, J.Y. Kresh, Cardiomyocyte-mediated contact programs human mesenchymal stem cells to express cardiogenic phenotype, J. Thorac. Cardiovasc. Surg. 126 (2003) 124–132.
[28] K.G. Gaustad, A.C. Boquest, B.E. Anderson, A.M. Gerdes, P. Collas, Differentiation of human adipose tissue stem cells using extracts of rat cardiomyocytes, Biochem. Biophys. Res. Commun. 31 (2004) 420–427.
[29] Y. Miyahara, N. Nagaya, M. Kataoka, et al., Monolayered mesenchymal stem cells repair scarred myocardium after myocardial infarction, Nat. Med. 12 (2006) 459–465.

Moriyama et al. BMC Cell Biology 2012, 13:21
http://www.biomedcentral.com/1471-2121/13/21

BMC Cell Biology

RESEARCH ARTICLE Open Access

Human adipose tissue-derived multilineage progenitor cells exposed to oxidative stress induce neurite outgrowth in PC12 cells through p38 MAPK signaling

Mariko Moriyama[1,2†], Hiroyuki Moriyama[1*†], Ayaka Ueda[1], Yusuke Nishibata[1], Hanayuki Okura[2], Akihiro Ichinose[3], Akifumi Matsuyama[2] and Takao Hayakawa[1]

Abstract

Background: Adipose tissues contain populations of pluripotent mesenchymal stem cells that also secrete various cytokines and growth factors to support repair of damaged tissues. In this study, we examined the role of oxidative stress on human adipose-derived multilineage progenitor cells (hADMPCs) in neurite outgrowth in cells of the rat pheochromocytoma cell line (PC12).

Results: We found that glutathione depletion in hADMPCs, caused by treatment with buthionine sulfoximine (BSO), resulted in the promotion of neurite outgrowth in PC12 cells through upregulation of bone morphogenetic protein 2 (BMP2) and fibroblast growth factor 2 (FGF2) transcription in, and secretion from, hADMPCs. Addition of *N*-acetylcysteine, a precursor of the intracellular antioxidant glutathione, suppressed the BSO-mediated upregulation of BMP2 and FGF2. Moreover, BSO treatment caused phosphorylation of p38 MAPK in hADMPCs. Inhibition of p38 MAPK was sufficient to suppress BMP2 and FGF2 expression, while this expression was significantly upregulated by overexpression of a constitutively active form of MKK6, which is an upstream molecule from p38 MAPK.

Conclusions: Our results clearly suggest that glutathione depletion, followed by accumulation of reactive oxygen species, stimulates the activation of p38 MAPK and subsequent expression of BMP2 and FGF2 in hADMPCs. Thus, transplantation of hADMPCs into neurodegenerative lesions such as stroke and Parkinson's disease, in which the transplanted hADMPCs are exposed to oxidative stress, can be the basis for simple and safe therapies.

Keywords: Human adipose-derived multilineage progenitor cells, Adult stem cells, Reactive oxygen species, p38 MAPK, Neurite outgrowth, BMP2, FGF2, Neurodegenerative disorders

Background

Mesenchymal stem cells (MSCs) are pluripotent stem cells that can differentiate into various types of cells [1-6]. These cells have been isolated from bone marrow [1], umbilical cord blood [2], and adipose tissue [3-6] and can be easily obtained and expanded *ex vivo* under appropriate culture conditions. Thus, MSCs are an attractive material for cell therapy and tissue engineering. Human adipose tissue-derived mesenchymal stem cells, also referred to as human adipose tissue-derived multilineage progenitor cells (hADMPCs), are especially advantageous because they can be easily and safely obtained from lipoaspirates, and the ethical issues surrounding other sources of stem cells can be avoided [4-6]. Moreover, hADMPCs have more pluripotent properties for regenerative medical applications than other stem cells, since these cells have been reported to have the ability to migrate to the injured area and differentiate into hepatocytes [4], cardiomyoblasts [5], pancreatic cells [7], and neuronal cells [8-10]. In addition, it is known that hADMPCs secrete a wide variety of cytokines and

* Correspondence: moriyama@phar.kindai.ac.jp
†Equal contributors
[1]Pharmaceutical Research and Technology Institute, Kinki University, 3-4-1 Kowakae, Higashi-Osaka, Osaka 577-8502, Japan
Full list of author information is available at the end of the article

growth factors necessary for tissue regeneration including nerve growth factor (NGF), brain-derived neurotrophic factor (BDNF), fibroblast growth factors (FGFs), vascular endothelial growth factor (VEGF) and hepatocyte growth factor (HGF) [11-14].

Recently, several groups have reported that hADMPCs facilitate neurological recovery in experimental models of stroke [9,10,15] and Parkinson's disease [16]. Despite the superiority of hADMPCs over other stem cells, the potential use of hADMPCs for the treatment of these neurodegenerative disorders has not been fully investigated. It has been reported that administration of hADMPCs in animal models of acute ischemic stroke markedly decreased brain infarct size, improved neurological function by enhancing angiogenesis and neurogenesis, and showed anti-inflammatory and anti-apoptotic effects [9,10]. These effects were due in part to increased secretion levels of VEGF, HGF and bFGF under hypoxic conditions [13], indicating the role of hADMPCs in reducing the severity of hypoxia-ischemic lesions.

In addition to hypoxic stress, ischemic lesions are generally subject to inflammation, which leads to the generation of reactive oxygen species (ROS) [17,18]. ROS are

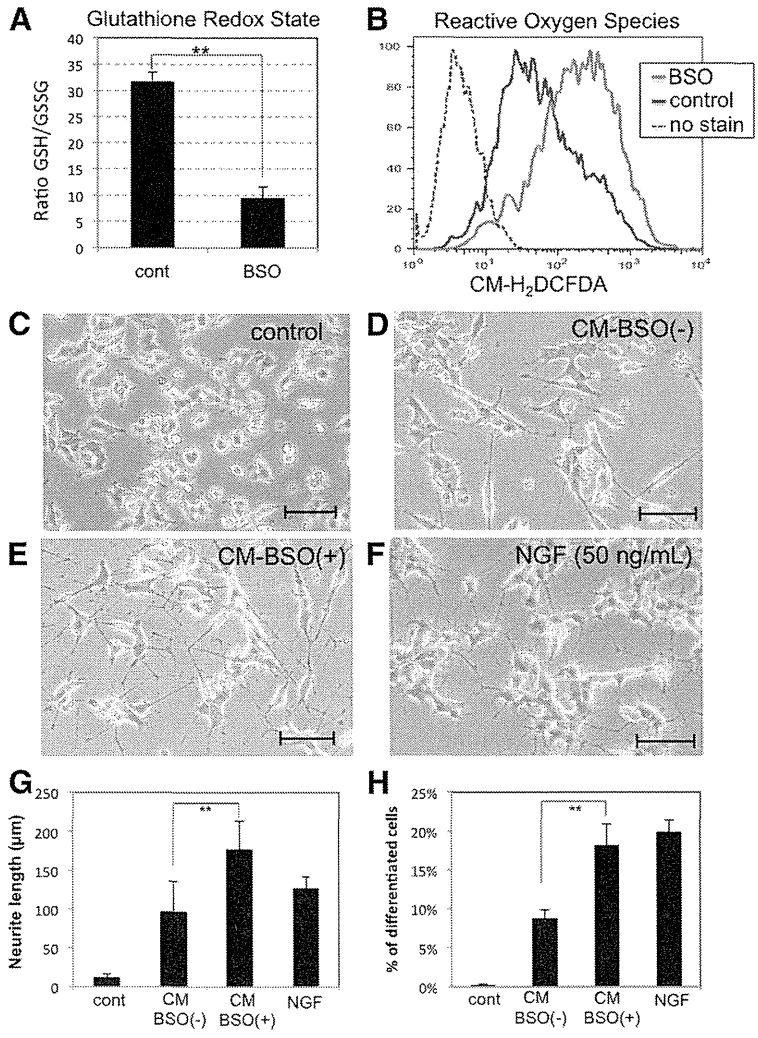

Figure 1 Conditioned medium from hADMPCs exposed to oxidative stress induces neurite outgrowth in PC12 cells. (A, B) Decrease of the reduced/oxidized glutathione ratios and increase in the intracellular ROS levels in hADMPCs treated with BSO. hADMPCs were treated with 1 mM BSO for 16 h, and cellular GSH/GSSG levels (**A**) or ROS (H_2O_2) levels (**B**) were analyzed. **(C-G)** Induction of neurite outgrowth in PC12 cells by conditioned medium from BSO-treated hADMPCs. PC12 cells were induced to differentiation by changing medium to differentiation medium alone (**C**), CM-BSO (–) (**D**), CM-BSO (+) (**E**), or differentiation medium with NGF (50 ng/mL) (**F**) for 2 days. Scale bars, 200 μm. (**G**) One hundred individual neurites were measured in each sample using Dynamic Cell Count Analyzer BZ-H1C (Keyence, Osaka, Japan) and average neurite length was calculated. **, $P < 0.01$ (Student's t test). **(H)** Percentage of neurite-bearing PC12 cells. A cell was scored positive for bearing neurites if it has a thin neurite extension that is double the length of the cell body diameter. A total of 500–600 cells in each sample were counted. **, $P < 0.01$ (Student's t test).

generated as a natural byproduct of normal aerobic metabolism, and mitochondrial respiration, together with oxidative enzymes such as plasma membrane oxidase, is considered to be the major intracellular source of ROS production [19]. Although appropriate levels of ROS play an important role in several physiological processes, oxidative damage initiated by excessive ROS causes many pathological conditions including inflammation, atherosclerosis, aging, and cancer. Neuronal cells are especially vulnerable to oxidative stress, and numerous studies have examined the crucial roles of oxidative stress in neurodegenerative disorders such as stroke [17,18], Alzheimer's disease [20,21], and Parkinson's disease [22,23]. In these diseases, microglia, the macrophages of the central nervous system (CNS), are activated in response to a local inflammation [24] and generate large amounts of reactive oxygen and nitrogen species, thereby exposing nearby neurons to stress [18,25]. Thus, the influence of oxidative stress generated by neurodegenerative lesion on hADMPCs needs to be further studied.

In this study, we examined the role of oxidative stress on hADMPCs in neurite outgrowth in cells of the rat pheochromocytoma cell line (PC12). Upon treatment with buthionine sulfoximine (BSO), an inhibitor of the rate-limiting enzyme in the synthesis of glutathione, hADMPCs accumulated ROS, which resulted in the upregulation of expression levels of the neurotrophic factors BMP2 and FGF2. Our present data thus provide new insights into understanding the mechanism of how hADMPCs exposed to oxidative stress contribute to neurogenesis, and this may explain the effects of stem cell transplantation therapy with hADMPCs in treating ischemic stroke.

Results

hADMPCs exposed to oxidative stress stimulate neurite outgrowth in PC12 cells

hADMPCs were treated with 1 mM BSO for 24 h; a group of hADMPCs that were not given any treatment was used as the control group. As shown in Figure 1A and B, BSO treatment resulted in significant reduction of intracellular reduced glutathione levels, followed by accumulation of intracellular reactive oxygen species (ROS) in hADMPCs. To investigate whether accumulation of ROS affects secretion of cytokines from hADMPCs, conditioned medium from BSO-treated (CM-BSO (+)) or BSO-untreated (CM-BSO (–)) hADMPCs was added to PC12 cells. As expected, addition of NGF significantly induced neurite outgrowth in the PC12 cells (Figure 1F, G, H). hADMPCs, like other mesenchymal stem cells derived from bone marrow or adipose tissue, may secrete many cytokines including NGF, BDNF and FGF2, and this may account for the slight induction of neurite outgrowth seen in the CM-BSO (–) treated cells (Figure 1D, G, H). In contrast, the number and length of neurite outgrowth of PC12 cells in CM-BSO (+) (Figure 1E) was markedly enhanced compared with those in CM-BSO (–) (Figure 1D, E, G, H).

Conditioned medium from BSO-treated hADMPCs activates Erk1/2 MAPK and Smad signaling in PC12 cells

To investigate which intracellular signaling pathways were involved in the neurite outgrowth of PC12 cells in CM-BSO (+), we used western blotting to determine the phosphorylation levels of Erk1/2 MAPK, p38 MAPK, Smad1/5/8 and Akt in PC12 cells in various culture conditions. NGF significantly activated Erk1/2 MAPK and Akt signaling pathway (Figure 2). In contrast, Erk1/2 MAPK was not activated in PC12 cells exposed to CM-BSO (–), while an increase in phosphorylated Smad1/5/8 was observed. Interestingly, CM-BSO (+) treatment led to both a significant increase in Smad1/5/8 phosphorylation levels as well as activation of the Erk1/2 MAPK

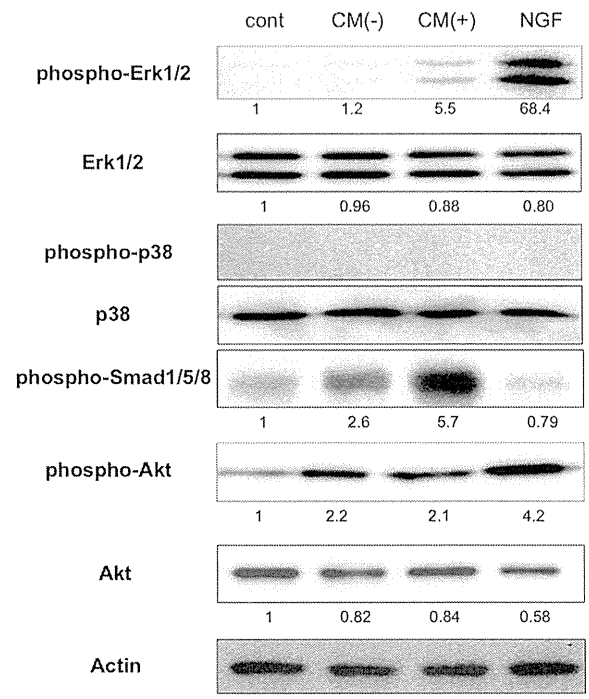

Figure 2 Erk1/2 MAPK and Smad1/5/8 are activated in PC12 cells cultured in conditioned medium from BSO-treated hADMPCs. Western blot analysis of PC12 cells cultured in differentiation medium alone (cont), CM-BSO (–), CM-BSO (+), or differentiation medium with NGF (50 ng/mL) for 1 h. Proteins extracted from each cell culture were resolved by SDS-PAGE, transferred to a membrane, and probed with anti-phosphorylated Erk1/2 (phospho Erk1/2), anti-Erk1/2, anti-phosphorylated p38 (phospho p38), anti-p38, anti-phosphorylated Smad1/5/8 (phospho Smad1/5/8), anti-phosphorylated Akt (phospho Ark) and anti-Akt. Actin was analyzed as an internal control. Numbers below blots indicate relative band intensities as determined by the ImageJ software.

signaling pathway in PC12 cells (Figure 2). Akt was 2-fold activated in both CM-BSO (–) and CM-BSO (+) treated PC12 cells, but no significant difference between the 2 groups was observed.

FGF2 and BMP2 are upregulated through p38 MAPK signaling in hADMPCs exposed to oxidative stress

We next examined which growth factors or cytokines from BSO-treated hADMPCs were involved in stimulation of neurite outgrowth. We found that both mRNA (Figure 3A and B) and protein (Figure 3C and D) levels for BMP2 and FGF2 were markedly increased in hADMPCs treated with BSO. To determine if this upregulation was caused by ROS, all cells were exposed to the antioxidant *N*-acetylcysteine (NAC). As we expected, addition of NAC to BSO-treated hADMPCs reduced the expression levels of BMP2 and FGF2 to control levels (Figure 3E and F). As BMP2 together with FGF2 has

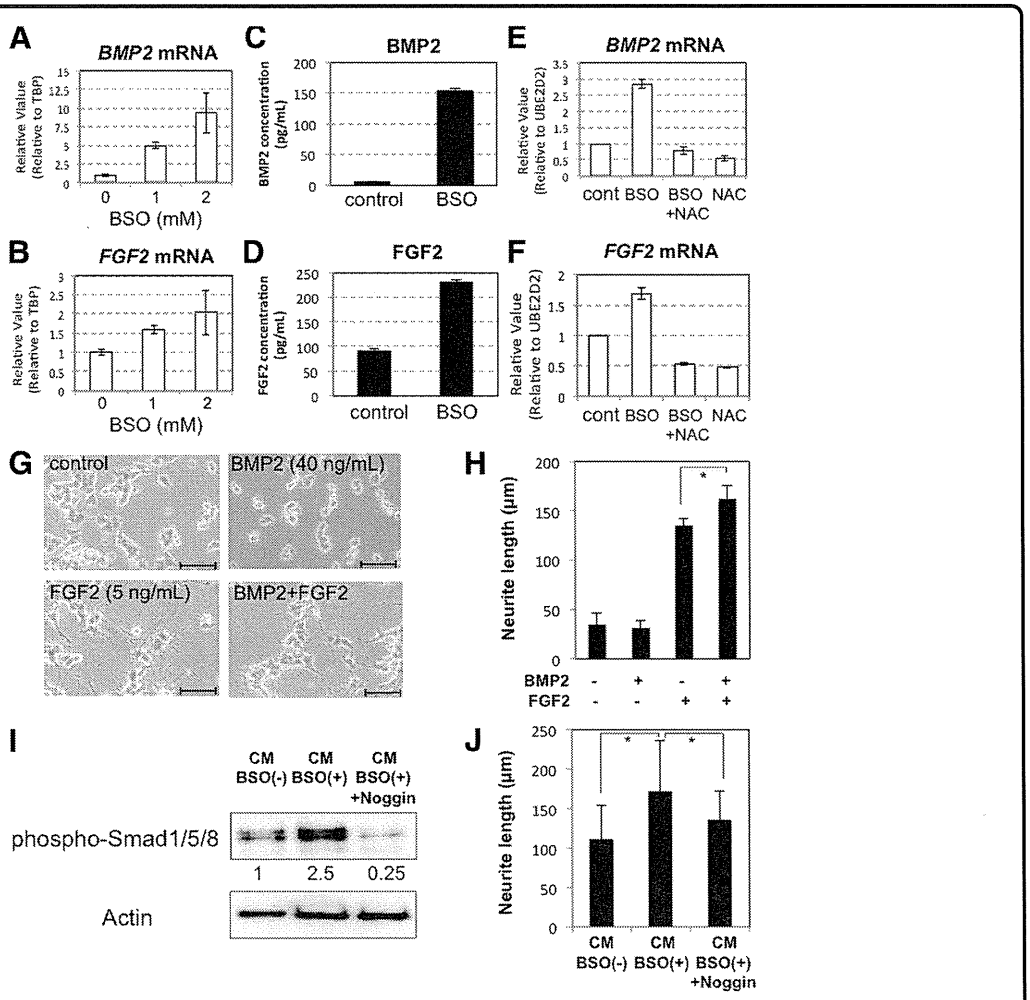

Figure 3 Transcription and secretion of BMP2 and FGF2 were increased in hADMPCs exposed to oxidative stress. (A, B) Upregulation of *BMP2* (**A**) and *FGF2* (**B**) mRNA in hADMPCs by BSO in a dose-dependent manner. **(C, D)** Secretion of BMP2 (**C**) and FGF2 (**D**) from hADMPCs in medium alone (cont) or with addition of 1 mM BSO (BSO) was analyzed by ELISA. **(E, F)** NAC treatment repressed the expression levels of *BMP2* and *FGF2* upregulated by BSO to the control levels. Expression of *BMP2* (E) and *FGF2* (F) mRNA was analyzed by q-PCR. cDNA was generated from total RNA extracted from hADMPCs (cont), hADMPCs treated with 1 mM BSO (BSO), 1 mM BSO + 5 mM NAC (BSO + NAC), and 5 mM NAC (NAC). The most reliable internal control gene was determined using the geNorm Software. **(G, H)** PC12 cells were cultured in differentiation medium alone (control), or differentiation medium supplemented with BMP2 (40 ng/mL), FGF2 (5 ng/mL), or both BMP2 and FGF2 (BMP2 + FGF2) for 2 days. (**G**) Representative images of neurite outgrowth in PC12 cells. Scale bars, 200 μm. (**H**) One hundred individual neurites were measured in each sample using Dynamic Cell Count Analyzer BZ-H1C (Keyence) and average neurite length was calculated. *, $P < 0.05$ (Student's t test). **(I, J)** PC12 cells were cultured in CM-BSO (–), CM-BSO (+), or CM-BSO (+) added with recombinant murine Noggin (200 ng/mL). **(I)** Western blot analysis of PC12 cells 1 h after CM treatment. Proteins extracted from each sample were resolved by SDS-PAGE, transferred to a membrane, and probed with anti-phosphorylated Smad1/5/8 (phospho-Smad1/5/8) and anti-Actin. Numbers below blots indicate relative band intensities as determined by the ImageJ software. (**J**) Two days after CM treatment, 100 individual neurites in PC12 cells were measured in each sample using Dynamic Cell Count Analyzer BZ-H1C (Keyence) and average neurite length was calculated. *, $P < 0.05$ (Student's t test).

previously been shown to induce neurite outgrowth in PC12 cells [26,27], we examined the effect of BMP2 and FGF2 on neurite outgrowth. We confirmed that PC12 cells did not differentiate effectively by BMP2 treatment alone, but BMP2 significantly augmented FGF2-induced neurite outgrowth in PC12 cells (Figure 3G and H), as previously reported. Moreover, in order to confirm the effect of BMP2 on neurite outgrowth in PC12 cells, 200 ng/mL of Noggin, an antagonist of BMP signaling, was added to CM-BSO(+). Addition of Noggin significantly suppressed the CM-BSO (+)-evoked phosphorylation of Smad1/5/8 (Figure 3I) and shortened the length of neurite outgrowth in PC12 cells (Figure 3J).

To address the question of which intracellular signaling pathways are affected by oxidative stress in hADMPCs, we focused on MAPK signaling since previous studies had suggested that accumulation of ROS in cells led to the activation of Erk1/2, p38, and JNK MAPK [28,29]. Western blotting revealed that BSO treatment markedly activated the p38 MAPK pathway; SB203580 could inhibit the activation, and U0126 treatment stimulated the activation (Figure 4A). ERK1/2 MAPK was significantly phosphorylated by BSO treatment, and ERK1/2 activation was reduced to the control level by treatment with U0126 (Figure 4B). In contrast, JNK activation was not observed in BSO-treated hADMPCs (Figure 4B). Therefore, we further investigated the relationship between increases in BMP2 and FGF2 expression and activation of the p38 and ERK1/2 MAPK signaling pathways by oxidative stress. Treatment

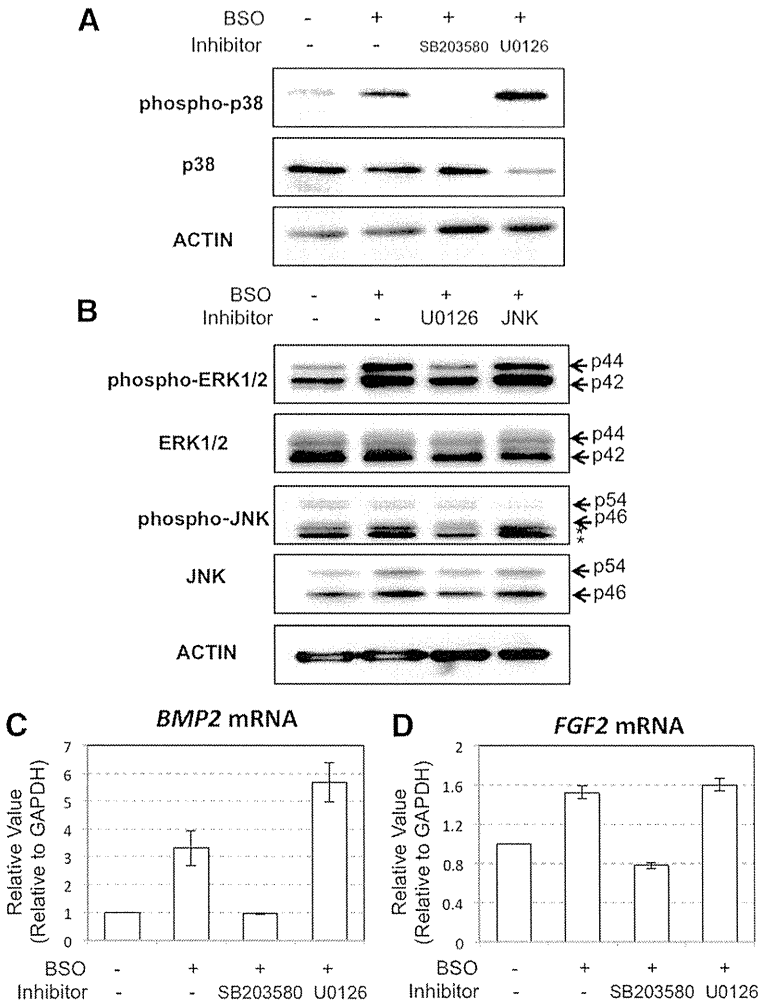

Figure 4 BMP2 and FGF2 were upregulated through activation of p38 MAPK. Inhibiton of p38 MAPK resulted in the supression of *BMP2* and *FGF2* transcripts upregulated by BSO treatment in hADMPCs. hADMPCs were pre-treated with 10 μM of SB203580, 10 μM of U0126 or 10 μM of JNK inhibitor II for 2 h followed by 1 mM BSO treatment for 16 h. The medium was replaced with fresh culture medium and the cells were cultured for another 2 days. **(A)** Western blot analysis of p38 MAPK activation in hADMPCs. **(B)** Western blot analysis of ERK1/2 MAPK, JNK SAPK activation in hADMPCs. **(C, D)** Transcription levels of *BMP2* (**C**) and *FGF2* (**D**) were analyzed by q-PCR. The most reliable internal control gene was determined using the geNorm Software.